International Journal of Nanomedicine

Dovepress
open access to scientific and medical research

Open Access Full Text Article

ORIGINAL RESEARCH

Multi-Modal Imaging Monitored M2 Macrophage Targeting Sono-Responsive Nanoparticles to Combat MRSA Deep Infections

Sijie Chen[1,2,*], Jiahao Wang[3–6,*], Kui Tang[1,2], Haiqin Liao[1,2], Yan Xu[1,2], Long Wang[3–6], Chengcheng Niu[1,2]

[1]Department of Ultrasound Diagnosis, the Second Xiangya Hospital, Central South University, Changsha, People's Republic of China; [2]Research Center of Ultrasonography, the Second Xiangya Hospital, Central South University, Changsha, People's Republic of China; [3]Department of Orthopedics, Xiangya Hospital, Central South University, Changsha, People's Republic of China; [4]Hunan Engineering Research Center of Biomedical Metal and Ceramic Implants, Xiangya Hospital, Central South University, Changsha, People's Republic of China; [5]National Clinical Research Center for Geriatric Disorders, Xiangya Hospital, Central South University, Changsha, People's Republic of China; [6]Hunan Key Laboratary of Aging Biology, Xiangya Hospital, Central South University, Changsha, People's Republic of China

*These authors contributed equally to this work

Correspondence: Chengcheng Niu, Department of Ultrasound Diagnosis, the Second Xiangya Hospital, Central South University, Changsha, 410011, People's Republic of China, Email niuchengcheng@csu.edu.cn

Background: MRSA with high morbidity and mortality is prone to cause serious infection, SDT has become a new antibiotic-free modality for bacterial infection treatment. Switching from proinflammatory M1 macrophages to anti-inflammatory M2 macrophages dominant could activate the immune system to generate an anti-infection immune response.

Methods: Herein, we developed M2 macrophages derived cell membranes coated PLGA nanoparticles with IR780 encapsulation (M2/IR780@PLGA) for antibacterial SDT and subsequent M2 macrophage polarization to enhance the therapeutic efficacy of MRSA myositis. For in situ visualization of antibacterial SDT, both diagnostic high-frequency US and magnetic resonance imaging (MRI) were introduced to monitor the sono-therapeutic progression of M2/IR780@PLGA nanoparticles in mice with bacterial myositis.

Results: Our developed M2/IR780@PLGA nanoparticles exhibited excellent antibacterial effects due to the IR780 under low-frequency US irradiation in vitro. In an MRSA-infected mice model, a great deal of M2/IR780@PLGA nanoparticles accumulated at the site of inflammation due to M2 macrophage coating. The infected legs in the M2/IR780@PLGA nanoparticles-based SDT group were significantly smaller, fewer blood flow signals, a slight muscular edema without obvious intermuscular abscesses under high-frequency US and MR images guidance. Histopathology proved the infected legs in the M2/IR780@PLGA nanoparticles-mediated SDT group had less clumped bacteria infiltration, more M2 macrophage expression and less M1 macrophage expression. The percentage of mature dendritic cells in spleens was much higher in the group of mice with M2/IR780@PLGA nanoparticles-based SDT.

Conclusion: This study provides a promising nanoparticles-based SDT anti-bacterial strategy, which could effectively enhance the antibacterial SDT and subsequent promote M2 macrophage polarization to boost the therapeutic efficacy of MRSA myositis.

Keywords: M2 macrophage, sonodynamic therapy, multidrug-resistant bacterial infections, antibacterial therapy, reactive oxygen species

Introduction

Methicillin-resistant Staphylococcus aureus (MRSA), as one of the multidrug-resistant (MDR) strain with high morbidity and mortality, is prone to cause serious infection which threatens public health.[1–3] Traditional antibiotic therapy is easy to induce drug resistance due to the overuse and misuse of antibiotics, resulting in poor long-term therapeutic effect.[4,5] In recent years, antibiotic-free antibacterial strategy as "nondrug" sterilization has been widely developed to combat the MDR infection.[6–10]

Received: 25 July 2022
Accepted: 13 September 2022
Published: 27 September 2022

Sonodynamic therapy (SDT) has become a new antibiotic-free modality for bacterial infection treatment, which utilizes low-frequency ultrasound (US) to play a part on a sonosensitizer and trigger the generation of cytotoxic reactive oxygen species (ROS) to kill bacteria without concerns about resistance.[11,12] Taking advantage of deep tissue-penetrating features of ultrasound wave, the deeply seated infections could be effectively suppressed, which is better than the penetration of photodynamic therapy (PDT).[13] The photosensitizers used in PDT usually could utilize as sonosensitizers, which could absorb US energy and be activated under US irradiation.[13,14] So far, some antibacterial sonosensitizers have been developed, including titanium dioxide (TiO_2), Ag, curcumin, and some porphyrin-based compounds.[15–17] IR780 iodide, as a cyanine dye with peak optical absorption at 780 nm wavelength, possesses the advantages of strong fluorescence intensity, excellent photothermal conversion efficiency, efficient US responsiveness, well inherent biosafety and low long-term toxicity, which render it good candidates for antibacterial therapy.[12,18–22] IR780-based nanomaterials used in antitumor SDT therapy were proven to be effective in inducing cancer cell death via ROS generation, while fewer studies were reported it used in antibacterial SDT therapy.[12,20] Our previous study demonstrated that IR780-based PLGA nanoparticles can effectively inhibit MRSA infection via singlet oxygen generation.[20]

In recent years, studies have found that macrophages play essential roles in tumor and inflammation immune microenvironment.[23,24] Macrophage phenotypes are often classified as classically activated M1 phenotype with proinflammatory function and alternatively activated M2 phenotype with anti-inflammatory function.[25,26] The macrophage phenotypes could switch in response to the various biochemical stimuli of local microenvironments and perform their functions dynamically.[27–30] The M2 macrophages are associated with inflammatory microenvironment and promote the process of inflammation relief, which are generally induced by the presence of anti-inflammatory cytokines, such as interleukin-4 (IL-4), IL-10, transforming growth factor-β (TGF-β) or glucocorticoids, and express high levels of arginase 1 (Arg 1), IL-10, CD163, CD204 or CD206.[23,31] CD206, also termed mannose receptor (MR), has been reported to be correlated with inflammatory diseases and induce macrophage activation.[32] Therefore, it is necessary to reprogram macrophages toward the M2 phenotype at appropriate time points in anti-infection therapy. Some scholars have found that nanoparticles with cell membrane modified on their surface can reduce their clearance by the immune system and ensure sufficient doses of nanoparticles to reach the target tissue.[33–37] Choo et al found that M1 macrophage-derived nanovesicles can target tumor tissues and repolarize M2 tumor-associated macrophages into M1 macrophages, thereby secreting proinflammatory factors and stimulating anti-tumor immune effects.[27] Increasing evidence has demonstrated that exosomes isolated from M2 macrophages can be used as drug carriers for the treatment of inflammatory diseases.[38,39] Li et al developed M2 exosomes derived from M2 macrophages as carriers for co-delivery of IL-10 plasmid DNA and chemotherapeutic drugs for the treatment of rheumatoid arthritis based on M1-to-M2 macrophage re-polarization.[38] Wu et al proved that engineered M2 exosomes exhibit excellent inflammation-tropism and anti-inflammation effects.[40] Pei et al provided an exosome membrane of M2 macrophages coated PLGA nanoparticles for the treatment of allergic asthma with good "homing" target to M2 macrophages in lung tissue.[41] However, M2 macrophage membranes derived nanoparticles targeted to infective tissue to polarize macrophages from M1 to M2 phenotype have rarely reported. Based on these, we propose to use M2 macrophage-derived cell membranes coating nanoparticles to target the inflammation microenvironment, induce the polarization of M1 macrophages into M2 macrophages and activate the anti-infection immune response.

In this study, we first developed M2 macrophages derived cell membranes coated PLGA nanoparticles with IR780 encapsulation (M2/IR780@PLGA) for antibacterial SDT and subsequent M2 macrophage polarization to enhance the therapeutic efficacy of MRSA myositis. For in situ visualization of antibacterial SDT, both diagnostic high-frequency US and magnetic resonance imaging (MRI) were introduced to monitor the sono-therapeutic progression of M2/IR780@PLGA nanoparticles in mice with bacterial myositis (Scheme 1). Thus, M2/IR780@PLGA nanoparticles could be used as efficient sono-responsive nanoparticles to enhance the antibacterial efficacy against MRSA deep infection.

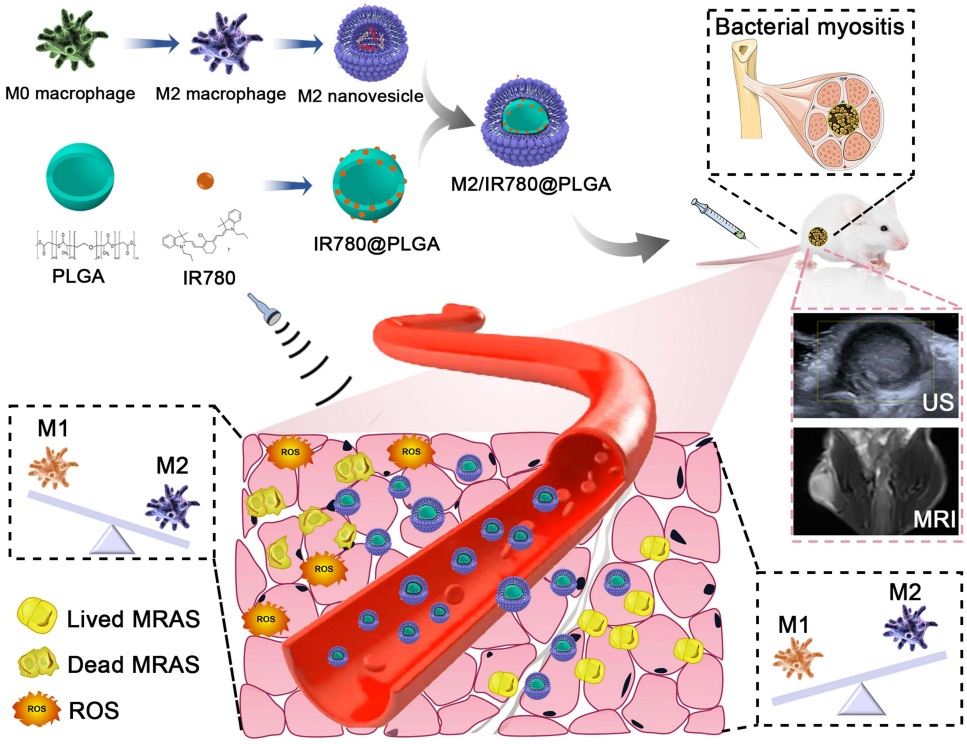

Scheme 1 Schematic illustration of the M2/IR780@PLGA nanoparticles for antibacterial SDT and subsequent M2 macrophages polarization to enhance the therapeutic efficacy of MRSA myositis, with dual-modal US and MRI monitoring the sono-therapeutic progression.

Materials and Methods

Materials

IR780 iodide, PLGA, and polyvinyl alcohol (PVA) were provided from Sigma Aldrich (St. Louis, MO, USA). Singlet Oxygen Sensor Green (SOSG) probe, IL-4, CD86 monoclonal antibody, CD80 monoclonal antibody, CD206 monoclonal antibody, and CD11c monoclonal antibody were purchased by Biolegend (San Diego, CA, USA). Cell-Counting Kit-8 (CCK-8), Calcein AM, 4, 6-diamidino-2-phenylindole (DAPI) and pyridine iodide (PI) were obtained from Beyotime Biotechnology (Shanghai, China). Staphylococcus aureus strains (MRSA, ATCC43300) and RAW 264.7 cell lines were obtained from Second Xiangya Hospital of Central South University (Changsha, China). All other reagents were of analytical grade and used without further purification.

Identification of M2 Macrophages

RAW 264.7 cells were cultured in Dulbecco's Modified Eagle Medium (DMEM) containing 10% fetal bovine serum (FBS) and 1% penicillin-streptomycin.[37] M2 macrophages were induced by the addition of 20 ng/mL IL-4 (Invitrogen, Carlsbad, CA).[27] To identify the conversion rate of M0 macrophages, CD206 on membranes was evaluated by flow cytometry analysis. M0 or M2 macrophages were collected and incubated with 1 μL of anti-CD206 antibody (Biolegend, USA) in the dark for 30 min, then fluorescence-labeled secondary antibodies (Yeasen, China) were added for 30 min, the precipitate was collected via centrifugation at 800 rpm and resuspended in 300 μL PBS. The stained cells were subjected to examination through a flow cytometer (BD FACSCelesta). To quantify the gene expression levels, macrophages were harvested and used for RNA extraction with the Trizol assay (Invitrogen, USA); then, the expressions of M2 (CD206, IL-10) markers were performed with real-time polymerase chain reaction (RT-PCR). The experiment was repeated three times, primer sequences used are listed in Table S1.

Preparation of M2/IR780@PLGA Nanoparticles

IR780@PLGA nanoparticles were prepared via a single emulsion evaporation protocol in the dark.[12,42,43] Briefly, 50 mg of PLGA and 1 mg of IR780 were completely dissolved in 2 mL of chloroform, 10 mL of PVA solution (cold, 4% w/v) was added to the above solution and emulsified for 2 min with an ultrasonic processor (Sonics, VCX150, USA). Then, 20 mL of deionized water was added to the emulsion and stirred for 3 h, the fabricated IR780@PLGA nanoparticles were collected and washed with deionized water by centrifugation for three times.

The IL-4 treated RAW 264.7 cells (M2 macrophages) were suspended in 1×PBS for 1h and then in 0.25×PBS for 1h at 4°C, the collected debris were spun down at 15000 rpm for 30 min, and extruded through polycarbonate membrane filters (Whatman) with pore size of 400 nm using a mini-extruder (Avanti Polar Lipids) to obtain M2 macrophage vesicles as described previously with minor improvement.[27,36,37] Then, 1 mL of IR780@PLGA nanoparticles (1 mg/mL) mixed with the M2 macrophage nanovesicles were sonicated for 30s to complete the membrane coating, the collected M2/IR780@PLGA nanoparticles were redispersed in 1×PBS after removing the excess M2 macrophage membranes by centrifugation.

Characterization of M2/IR780@PLGA Nanoparticles

The structures of IR780@PLGA nanoparticles, M2 macrophages derived vesicles and M2/IR780@PLGA nanoparticles were examined by transmission electron microscopy (TEM, Hitachi H-7600). The size distributions and zeta potentials of M2/IR780@PLGA nanoparticles and IR780@PLGA nanoparticles were tested by a dynamic light scattering (DLS) analyzer (Malvern Nano ZS, UK). Stability experiments of M2/IR780@PLGA nanoparticles were measured in 1 × PBS or in 10% FBS with DLS over 7 days. The existence of IR780 in the M2/IR780@PLGA nanoparticles was used by a UV-Vis-NIR spectrophotometer (Cary 5000, USA) and the IR780 loading was calculated according to the following equation:[44]

$$\text{Encapsulation efficiency}(\%) = \frac{\text{Weight of IR780 in the nanoparticles}}{\text{Weight of total added IR780}} \times 100\% \quad (1)$$

To confirm the spatial colocalization of M2 macrophages derived vesicles (DiO-labeled green fluorescence) and IR780@PLGA nanoparticles (DiI-labeled red fluorescence), the colocalization fluorescence images of M2/IR780@PLGA nanoparticles were carried out by a confocal laser scanning microscopy (CLSM, Carl Zeiss, LSM 510 META).

The production of singlet oxygen ($^1O_2$) was measured using SOSG as a fluorescent probe, 100 μL of M2/IR780@PLGA nanoparticles (20 mg/mL) solution and 1 μL of SOSG (2.5 mM) were mixed in a quartz cuvette. A low-frequency US transducer (WED-100, WELLD Medical Electronics, China) was used for irradiated the production of $^1O_2$ (1 MHz, 2 W/cm^2, 40% duty cycle) for 0, 30, 60, 90, 120, or 150 s, and then the fluorescence spectra of SOSG were acquired on a fluorescence spectrometer with an excitation wavelength of 504 nm.

Minimum Inhibitory Concentration (MIC) Test

For bacteria recovery, Staphylococcus aureus strain ATCC 43300 was inoculated on Tryptic Soy Agar after streaking out from −80°C glycerol stocks.[45] After incubation at 37°C for 24 hours, one colony was picked out to dissolve with 2mL tryptic soy broth (TSB) culture medium, which was streaked out again on Tryptic Soy Agar plates. After 16 hours, active colonies were selected to dissolve into 5mL TSB broths until the medium absorbance reached 0.5 at OD_{600nm} (the optical density at a wavelength of 600 nm). To explore the effect of ultrasound on bacterial growth, five aliquots of 1:100 dilution of the suspension were made. One mL per tube of bacterial solution was added into five 1.5mL Eppendorf tubes (EP) tubes, which received 0W/cm^2, 0.5W/cm^2, 1W/cm^2, 1.5W/cm^2, and 2W/cm^2 ultrasound (US) administration, respectively, for 4 on/off cycles (1 MHz, 30 seconds on and 30 seconds off in each cycle). After that, the bacteria were incubated at 37°C for 18 hours. To explore the effect of nanoparticles with US on bacterial growth, twelve aliquots of 1:100 dilution of the suspension were made. The M2/IR780@PLGA nanoparticles were prepared by diluting the original 10mg/mL nanoparticle suspension in PBS, 500 μL each of these bacterial dilutions and 500 μL of M2/IR780@PLGA nanoparticles were added together into a 1.5 mL EP tube, with final nanoparticle concentrations at 0

μg/mL, 100 μg/mL, 200 μg/mL, 300 μg/mL, 400 μg/mL, and 500 μg/mL. The experiment groups were set as follows: M2/IR780@PLGA nanoparticles treated: 0 μg/mL (control), 100 μg/mL, 200 μg/mL, 300 μg/mL, 400 μg/mL, and 500 μg/mL; M2/IR780@PLGA+US treated: 0 μg/mL (control), 100 μg/mL, 200 μg/mL, 300 μg/mL, 400μg/mL, and 500μg/mL. M2/IR780@PLGA+US treated groups received 2W/cm^2 of US treatment for 4 on/off cycles (30 seconds on and 30 seconds off in each cycle). After that, the bacteria and serially diluted nanoparticles were incubated at 37°C for 18 hours. After incubation, the growth of bacteria was judged by measuring the turbidity of tubes at OD_{600nm} with a microplate spectrophotometer (BioTek Epoch, China). The experiment was repeated for 3 times in different days. For each experiment, there were three duplicate tubes in each treated group.

Biofilm Inhibition and Destruction Test

Active bacteria colony was dissolved in TSB broths containing 0.5% glucose (w/v) as described above to reach 0.1 OD_{600nm} absorbance. The M2/IR780@PLGA nanoparticles were also diluted with TSB broths containing 0.5% glucose (w/v). Experiment groups were designed as the above.

For biofilm inhibition test, 100 μL per well of nanoparticles and 100 μL per well of bacteria suspension were added together into a flat bottom polystyrene 96 well plate. In US-treated group, the bacteria suspension received US treatment immediately after addition of nanoparticles. The plates were then incubated statically in an incubator at 37°C for 24 hours. After incubation, the suspension was carefully removed. The plates were washed twice with 100 μL per well of PBS and left to dry at room temperature for 30 minutes. When removing or adding liquids from or into the wells, tips were inserted slowly to avoid touching the biofilm. Biofilms were then fixed with 100 μL per well of anhydrous ethanol for 30 min at room temperature and dried under flowing air. Then, 100 μL per well of 0.1% v/v crystal violet was added into the plates to stain the biofilm at room temperature. Fifteen minutes later, the plates were washed under slowly running tap water until the water became clear. The plates were left under flowing air to dry. Pictures were taken to observe biofilms' formation and 200 μL per well of anhydrous ethanol was added into the well to elute the stain for 30 minutes at room temperature. One hundred μL per well of the eluent was transferred into a new 96-well plate and the absorbance was measured at OD_{590nm} using spectrophotometer.[46]

For biofilm destruction test, no US treatment was administrated before mature biofilms formed, 100 μL per well of bacteria suspension was added into a flat bottom polystyrene 96 well plate and incubated statically in an incubator at 37°C for 24 hours, to form mature biofilms. And then bacteria suspension was removed carefully and 100 μL per well of nanoparticles were added into biofilms. For US-treated groups, US treatment was immediately administrated after addition of nanoparticles. After that, the nanoparticles-treated biofilms were cultured at 37°C for 24 hours. After incubation, biofilms were washed, air-dried, stained and eluted to quantify as described in biofilm inhibition test. Both inhibition and destruction tests were repeated for 3 independent times in different plates at different days. For each experiment group, there were three independent wells.

Observation of Biofilm by Fluorescence Microscopy

Bacteria suspension was treated with equal volume of nanoparticles and received US treatment or not, as described in the above biofilm inhibition test, 500 μL per well of bacteria suspension and 500 μL per well of nanoparticles were added together into confocal dishes. After treatment, the dishes were incubated at 37°C for 24 hours to form mature biofilm. The suspension was removed gently. The biofilms were washed twice with PBS and stained with Calcein-AM/PI Double Stain Kit (YEASEN, China) at 37°C for 15 minutes. The biofilms were stained with green fluorescence and observed in a Leica fluorescence microscope (Leica MICROSYSTEMS) and CLSM. ImageJ software was used to quantify the biofilms. The experiment was repeated in different dishes for 3 independent times at different days.

Cell Leakage Test

Active colonies were selected after recovery and dissolved into 10 mL TSB broths. The broths were shaken in an incubator shaker at 37°C for 24 hours, and later certificated at 8000×g for 10 minutes. Pellets were washed twice by resuspending them again with PBS and certificated. Then, pellets were resuspended with PBS and divided into aliquots in twelve EP tubes. Each aliquot was subjected to nanoparticles and US treatment as described above. Nanoparticles were

serially diluted with PBS. Six hours after the treatment, samples were certificated at 10,000×g for 12 minutes. Pellets were prepared for scanning electron microscope (SEM, JSM-7800F, JEOL, Japan) examination. The supernatant was collected for cell leakage examination. Leaked nucleic acids was measured at OD_{260nm}. Leaked proteins were detected by BCA (Bicin-choninic Acid) Protein Assay Kit (New Cell & Molecular Biotech Co., Ltd).[47] Briefly, the working fluid was prepared by mixing BCA-A Solution and BCA-B Solution at a volume ratio of 50:1. 200 μL of the working fluid and 20 μL of the supernatant were added together into a 96 well-plate and incubated at 37°C for 30 minutes. Later, the absorbance was measured at OD_{562nm} using spectrophotometer. The experiment was repeated for 3 independent times at different days.

Morphology Observation of Bacteria by Scanning Electron Microscope

Pellet samples were obtained in 1.5 mL EP tubes as described in the cell leakage test, 1.2 mL per tube of 4°C pre-cooled fixative (1 mL 25% glutaraldehyde aqueous solution, 5 mL 0.2M phosphate buffer (pH7.0), and 4 mL distilled water in every 10 mL fixative) was slowly added into tubes along the tube wall to fix samples at 4°C overnight. After that, samples were rinsed with PBS for three times, 15 minutes each time, and fixed with 1% osmic acid solution for 2 hours. After fixation, samples were washed with PBS and dehydrated with ethanol solutions of gradient concentrations (including 30%, 50%, 70%, 80%, 90% and 95%). For each concentration, samples were treated for 15 minutes, and then treated with 100% ethanol twice, 20 min each time. After that, samples were treated with a mixture of ethanol and isoamyl acetate (V/V=1/1) for 30 minutes, and then with pure isoamyl acetate for 1 hour. Finally, after critical point drying and coating, the processed samples were observed by SEM. The experiment was repeated for 3 independent times at different days.

Detection of Bacterial $^1O_2$ Production

Bacteria were treated with nanoparticles and US as described above, $^1O_2$ generation was detected by ROS assay kit (Beijing Boxbio Science & Technology Co., Ltd.). Briefly, active colonies were selected to dissolve into 5 mL TSB broths until the medium absorbance reached 0.5 at OD_{600nm}, 1 mL per well of 1:5 dilution of the bacterial suspension was inoculated in a flat 6-well plate and cultured statically in an incubator at 37°C for 24 hours. After incubation, bacterial suspension was removed and attached bacteria were gently washed three times with PBS. Then, 1 mL per well of 10 μmol/L DCFH-DA probe (10 μmol/L, diluted in serum-free medium) was added into the plate and incubated with bacteria at 37°C for 20 minutes. After incubation, unloaded probe was eluted with PBS and bacteria were treated with nanoparticles and US. Intracellular $^1O_2$ can oxidize DCFH to generate fluorescent DCF, which could be detected with green fluorescence under 480 nm excitation light. Finally, bacteria were washed with PBS for three times and observed in a Leica fluorescence microscope. Besides, active colonies were selected to dissolve into 5 mL PBS until the suspension absorbance reached 0.5 at OD_{600nm}, 12 mL of 1:5 dilution of the bacterial suspension was incubated with 12 μL of DCFH-DA probe at 37°C for 20 minutes. After that, bacteria loaded with probe were collected by certification at 8000×g for 10 minutes and washed with serum-free medium for three times to remove the unloaded DCFH-DA. Bacteria were then resuspended with PBS, divided into 12 aliquots and treated with nanoparticles and US, 100 μL per well of treated bacterial suspension was then transferred into a new flat 96-well plate. Fluorescent intensity of the suspension was detected by EnVision® 2105 Multimode Plate Reader (PerkinElmer, China) under 480 nm excitation light. The experiment was repeated for 3 independent times at different days.

In vivo Imaging of Bacterial Infections

Female BALB/c mice (5 weeks old, 20 g) were obtained from the Medical Experimental Animal Center of the Second Xiangya Hospital, Central South University (Changsha, China). The right thighs of the mice were shaved and intramuscularly injected with 50 μL of MRSA bacterial solution (1×10^9 CFU/mL). The bacterial infection models were successfully established 3 days later, when the thigh skin showed redness and swelling. All animal experiments were approved by the Ethics Committee of the Second Xiangya Hospital of Central South University and conducted in accordance with the guidelines of the Department of Laboratory Animals of Central South University.

To evaluate the targeting property of M2/IR780@PLGA nanoparticles at infected lesion, the in vivo fluorescence images were acquired by a Lumina IVIS Spectrum imaging system (PerkinElmer, USA). Bacterially infected mice were

intravenously injected with 200 μL of M2/IR780@PLGA nanoparticles or IR780@PLGA nanoparticles (10 mg/mL), and imaged in vivo at different time points (4h, 12h, 24h, 36h, 48h, 72h, 96h and 108h after injection). Then, the legs and major organs were harvested and imaged for ex vivo fluorescence at 24h, and the average in vivo and ex vivo fluorescence intensities were calculated.

In vivo Antibacterial SDT of MRSA Infections

To evaluate the antibacterial SDT efficacy of M2/IR780@PLGA nanoparticles, bacterial-infected mice were divided into four groups (n = 5): 1) M2/IR780@PLGA + US group, 2) IR780@PLGA + US group, 3) US group, and 4) saline group. The mice in groups 1 and 2 were intravenously injected with 200 μL of M2/IR780@PLGA or IR780@PLGA nanoparticles (10 mg/mL) at 0, 3, 6, 9 and 12 days. The mice in groups 1, 2 and 3 were exposed to US irradiation (1 MHz, 2.0 W/cm^2, 30s on and 30s off for four on/off cycles, 4 min in total) at 1, 4, 7, 10 and 13 days. To further assess the treatments in visualization, both the B-mode and CDFI-mode ultrasound images of the legs were acquired on a portable US apparatus Vinno 8 (VINNO, Suzhou, China) at different time points (0, 4, 9, and 14 days), and the body weights were also measured at these time points.[20] At the 14 days, all mice were carried out the MR imaging for the legs, and then the legs were harvested for hematoxylin and eosin (H&E) and Giemsa staining to assess the bacterial contamination of the MRSA myositis. Additionally, the immunofluorescence histology was performed for the immune microenvironment (CD206, CD86 and IL-10) of the MRSA myositis to qualitatively and quantitatively estimate the M1 or M2 macrophages. Blood samples were collected for serum biochemical assays at days 0 and 14 to evaluate the serum inflammatory levels, including C-reactive protein (CRP), neutrophil cells and white blood cells (WBC).

Immune Responses Induced by Antibacterial SDT of MRSA Infections

To evaluate the immune responses induced by antibacterial SDT efficacy of M2/IR780@PLGA nanoparticles, bacterial-infected mice were divided into four groups (n = 3): 1) M2/IR780@PLGA + US group, 2) IR780@PLGA + US group, 3) US group, and 4) saline group. After different treatments 14 days in each group, the spleens were harvested and stained with anti-CD80-PE, anti-CD86-APC and anti-CD11c-FITC antibodies according to the manufacturer's protocols[48] by flow cytometry.

Safety Assessment of M2/IR780@PLGA Nanoparticles

For assessment of the biological toxicity of the developed M2/IR780@PLGA nanoparticles, 20 female BALB/c bacterial-infected mice were divided into 4 groups: 1) M2/IR780@PLGA + US group, 2) IR780@PLGA + US group, 3) US group, and 4) saline group. Five healthy mice were used as control. Blood samples were collected for serum biochemistry assays at 14 days after different treatments, including alanine aminotransferase (ALT), aspartate aminotransferase (AST), urea nitrogen (UREA) and creatinine (CREA). After sacrifice at the final time point, the major organs including the heart, liver, spleen, lung and kidney were harvested for H&E staining to access the histological changes.

Statistical Analysis

All data are presented as means ± standard deviation (SD), One-way ANOVA and Student's *t*-test was used to analyze the data. Value of $*p < 0.05$ was considered statistically significant.

Results and Discussion

Preparation and Characterization of M2/IR780@PLGA Nanoparticles

In this study, we prepared M2/IR780@PLGA nanoparticles for antibacterial SDT and subsequent M2 macrophage polarization to enhance the therapeutic efficacy of MRSA myositis. M2/IR780@PLGA nanoparticles was facilely synthesized via a single emulsion evaporation and well-established "top-down" method[36] (Figure 1A). M2 macrophages were induced by the addition of 20 ng/mL IL-4, to identify the M2 polarized macrophages, CD206 on membranes and RNA expression levels (CD206 and IL10) were evaluated by flow cytometry analysis and RT-PCR analysis, respectively.

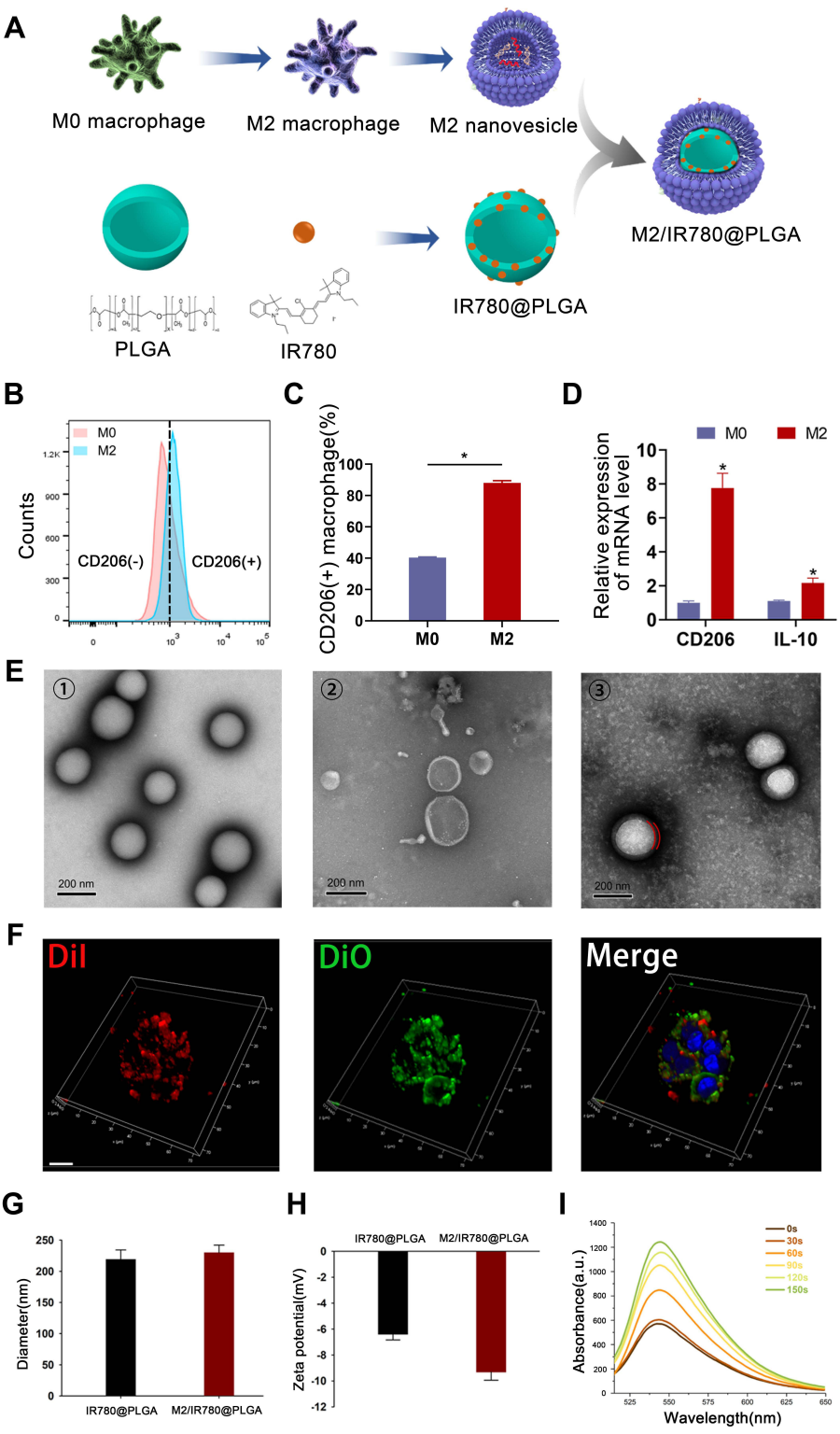

Figure 1 Characterization of M2/IR780@PLGA nanoparticles.

Notes: (**A**) Schematic illustration of the preparation of M2/IR780@PLGA nanoparticles. (**B-D**) Definition of M2 polarized macrophages by (**B**) flow cytometry and (**C**) quantification results. (**D**) Induction of macrophage switching from M0 to M2 by IL-4, RNA expression levels of CD206 and IL-10 in macrophages determined by quantitative real-time polymerase chain reaction. Statistical significances were calculated via Student's *t* test, $^{*}p < 0.05$. (**E**) The TEM image of ① IR780@PLGA nanoparticles (Scale bar: 200 nm), ② M2 nanovesicles (Scale bar: 200 nm) and M2/IR780@PLGA nanoparticles (Scale bar: 100 nm). (**F**) Typical confocal images of RAW264.7 incubated with M2/IR780@PLGA nanoparticles (DII-labeled IR780@PLGA nanoparticles (red) and DiO-labeled M2 nanovesicle (green)). Scale bar, 10 μm. (**G**) Size and (**H**) zeta distributions of IR780@PLGA nanoparticles and M2/IR780@PLGA nanoparticles. (**I**) Time-dependent $^{1}O_2$ generation of M2/IR780@PLGA nanoparticles using SOSG as a fluorescence probe with US irradiation (1 MHz, 2.0 W/cm^2).

As shown in Figure 1B and C, after induction by IL-4, the M2 polarized macrophages expressed the CD206 more than 80%, which was obviously higher than the M0 macrophages (expressed only 40% of CD206). Then, RNA expression levels of CD206 and IL-10 in macrophages determined by quantitative RT-PCR. As shown in Figure 1D, the expression level of CD206 in M2 macrophages was more than 7-fold to M0 macrophages, and the expression level of IL-10 in M2 macrophages was almost 2-fold to M0 macrophages, which means the M2 macrophages were successfully polarized from M0 macrophages. These results demonstrated that after induction by IL-4, most of M0 macrophages were successfully polarized to M2 macrophages. The developed M2/IR780@PLGA nanoparticles disappeared an aquamarine color, compared with the light green color of IR780@PLGA nanoparticles, which successfully color (Figure S1). The UV-vis-NIR absorption spectra confirmed the existence of IR780, endowing the M2/IR780@PLGA nanoparticles could be used as a good sonodynamic agent (Figure S2). The standard curve of IR780 was calculated and the encapsulation efficiency of IR780 was 57.61 ± 4.53% (Figure S3). The structure of M2/IR780@PLGA nanoparticles was observed by TEM examination, as shown in Figure 1E, the naked IR780@PLGA have a uniform spherical shape (Figure 1E①), the M2 macrophage nanovesicles have a uniform vesicle-like shape (Figure 1E②). After M2 macrophage nanovesicles coating, all M2/IR780@PLGA nanoparticles revealed the expected core–shell structures with the M2 macrophage membrane as the outer shell, and the thickness of the outer shell was about 15–20 mm (Figure 1E③). Following the structural studies, the DiI-labeled red fluorescence indicated IR780@PLGA nanoparticles (Figure 1F①) and DiO-labeled green fluorescence indicated M2 macrophages derived vesicles (Figure 1F②) were colocalized in the M2/IR780@PLGA nanoparticles. Most of the green fluorescence and red fluorescence were overlaid in the merged image, indicating the M2 macrophages derived vesicles were successfully coated on the IR780@PLGA nanoparticles (Figure 1F③). Following M2 macrophage membrane coating, the average diameter of the M2/IR780@PLGA nanoparticles changed from 220 to 235 nm (Figure 1G), and the surface zeta potential of the M2/IR780@PLGA nanoparticles changed from −6.3 to −9.2 mV (Figure 1H). These results suggested that the M2 macrophage membranes were successfully coated on the IR780@PLGA nanoparticles. In addition, insubstantial changes were found in the size and zeta potential of M2/IR780@PLGA nanoparticles over 7 days in PBS and 10% FBS monitored by DLS, suggesting that the M2/IR780@PLGA nanoparticles have a remarkable colloidal stability, which makes it potential sono-therapeutic agent for in vivo study (Figure S4). Then, SOSG was applied to confirm $^1O_2$ generation in vitro based on fluorescence intensity to explore the potential of the M2/IR780@PLGA nanoparticles as a sonosensitizer. As displayed in Figure 1I, the fluorescence intensity of the SOSG solution (2.5 mM) containing M2/IR780@PLGA nanoparticles (20 mg/mL) increased drastically with prolonged US irradiation (1MHz, 2 W/cm^2), the fluorescence intensity increased more than 2-fold within 150 s. These results indicated the M2/IR780@PLGA nanoparticles have potential sonosensitizers for antibacterial SDT after M2 macrophage coating.

MIC Test in vitro

To explore the effect of ultrasound or nanoparticle intensities on bacterial growth, MIC test was carried out. Plate counting results of ATCC 43300 strain treated with M2/IR780@PLGA nanoparticles proved that the bacterial growth obviously inhibited at high concentrations more than 500 μg/mL, MIC test results of ATCC 43300 strain treated with M2/IR780@PLGA nanoparticles indicated the nanoparticles started to inhibit bacterial growth at 100 μg/mL, and have significant anti-bacterial growth effect when the concentrations of nanoparticles as high as 500 μg/mL (Figure S5). Figure 2 presents the antibacterial effects of ultrasound and M2/IR780@PLGA nanoparticles on MRSA ATCC43300 strain. Figure 2A and B demonstrated that ultrasound had no obvious inhibition effect on bacterial growth at different intensities, while M2/IR780@PLGA nanoparticles could play a bactericidal effect dose-dependently. Nanoparticles started to inhibit bacterial growth at 100 μg/mL and inhibited more than 90% ATCC43300 strain at concentrations of 400 μg/mL and 500 μg/mL. Moreover, with the combination of M2/IR780@PLGA nanoparticles and ultrasound, nanoparticles performed obviously improved bactericidal effect, even though 100 μg/mL nanoparticles with ultrasound could inhibit more than 90% bacterial growth compared with the control group, which indicating that M2/IR780@PLGA nanoparticles could effectively inhibit ATCC43300 strain growth. The application of ultrasound further enhanced the bactericidal action of nanoparticles, which should be contributed to the combination of ultrasound and nanoparticles, instead of ultrasound alone.

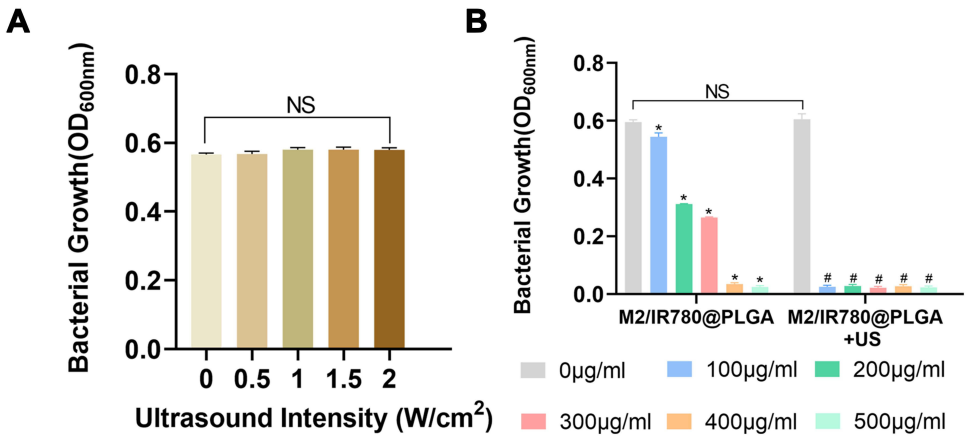

Figure 2 The MIC results of ATCC43300 strain treated with (**A**) ultrasound and (**B**) M2/IR780@PLGA nanoparticles (administrated with or without ultrasound).
Notes: The results are presented as the average of three independent experiments and analyzed by One-way ANOVA. *p < 0.05 means statistically significant difference between M2/IR780@PLGA nanoparticles treated groups and control group; #p < 0.05 means statistically significant difference between M2/IR780@PLGA nanoparticles with ultrasound treated groups and control group. NS means no statistically significant difference between compared groups.

Biofilm Inhibition and Destruction Test

Figure 3 shows the effects of M2/IR780@PLGA nanoparticles and ultrasound on ATCC43300 strain biofilm. Figure 3A shows the results of biofilm inhibition and destruction test through crystal violet staining tests. Biofilm inhibition test (above) showed that M2/IR780@PLGA nanoparticles could dose-dependently inhibit the biofilms formation. The inhibition was enhanced with administration of ultrasound. As can be seen from Figure 3C (a), 100 μg/mL could slightly inhibit biofilm formation, 200 μg/mL nanoparticles could inhibit more than 90% biofilm formation. Furthermore, with the assistance of ultrasound, all groups could inhibit biofilm formation more than 90%. Biofilm destruction test (below) showed that, M2/IR780@PLGA nanoparticles alone could not destroy formed biofilms, however, performing obvious destruction effect on biofilms after the administration of ultrasound, which is shown in Figure 3C (b). The quantification showed significant difference between ultrasound alone treated group and non-ultrasound group, while no difference between different nanoparticle concentration groups, which indicated that the biofilm destruction effect mainly contributed to ultrasound. Fluorescence microscopy was further adapted to observe biofilm formation after nanoparticles' treatment, as shown in Figure 3B. The 3D images of biofilm formation after nanoparticles' treatment were also carried by CLSM for overall observation (Figure S6). Biofilm formation was decreased in 100 μg/mL group compared with 0 μg/mL group, and inhibited more than 90% in other concentration groups. The inhibition effect was also strengthened by ultrasound, which is quantified in Figure 3C (c) and kept consistent with the crystal violet staining test. Figure 3 proves that M2/IR780@PLGA nanoparticles could effectively inhibit biofilm formation, especially when nanoparticle concentration was more than 200 μg/mL. Ultrasound could obviously enhance the ability of M2/IR780@PLGA nanoparticles in biofilm formation, M2/IR780@PLGA nanoparticles alone could not destruct the formed biofilms on plates. However, ultrasound could obviously destroy formed biofilms.

Cell Leakage Test, SEM and $^1O_2$ Generation

Given that M2/IR780@PLGA nanoparticles with ultrasound effectively inhibited bacterial growth and biofilms, further mechanisms are explored in Figure 4. Intact membranes are essential for bacterial survival. Disruption of bacterial membrane integrity will cause cell content release and bacterial death.[49] Therefore, cell leakage test was adapted to detect the protein and nucleic acid contents released from bacteria cells.[50] As can be seen from Figure 4A (a) and (b), both of nucleic acid and protein contents released from bacteria increased dose-dependently after M2/IR780@PLGA nanoparticle treatment, with or without ultrasound, which indicated that the cell membrane integrity was broken by nanoparticles. Comparing non-ultrasound and ultrasound treated groups, we could see in Figure 4A (c) and (d) that ultrasound significantly augmented nanoparticles' effect on bacterial cell membrane disruption. However, ultrasound alone treatment showed no difference with control group. It indicated that ultrasound alone would not affect the bacterial cell membrane

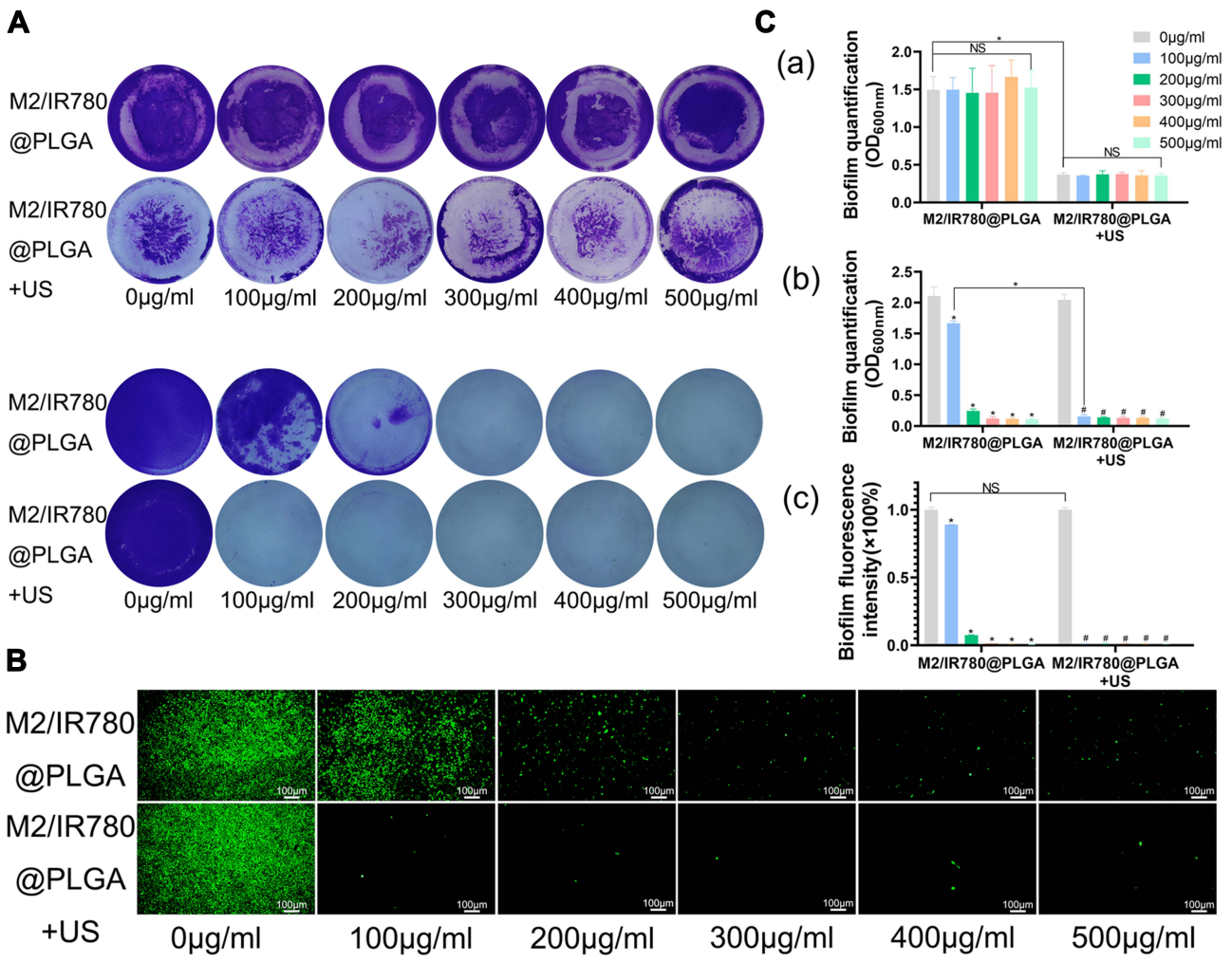

Figure 3 Biofilm inhibition and destruction test.

Notes: (**A**) Crystal violet staining results of biofilms formation (above) and destruction (below) after treated with M2/IR780@PLGA nanoparticles with or without ultrasound treatment. (**B**) The inhibition effect of M2/IR780@PLGA nanoparticles on biofilms formation observed by fluorescence microscopy. (**C**) Quantifications of biofilms inhibition, biofilms destruction, and fluorescence observation are shown in (a), (b), and (c), respectively. The quantification results are the mean of three independent experiments and analyzed by One-way ANOVA. *$p < 0.05$ means statistically significant difference between M2/IR780@PLGA nanoparticles treated groups and control group; #$p < 0.05$ means statistically significant difference between M2/IR780@PLGA nanoparticles with ultrasound treated groups and control group. NS means no statistically significant difference between compared groups.

integrity, instead, promoting M2/IR780@PLGA nanoparticles in destroying bacterial cell membrane integrity. In addition, SEM was used to observe the bacterial macrophage changes. As shown in Figure 4B, with the increased concentration of M2/IR780@PLGA nanoparticles, bacterial cell membrane began to collapse and the cells shrank, especially in the high concentration group, 500 μg/mL. After combination with ultrasound, bacterial cells in 100 μg/mL group performed apparent shrink. Bacterial cells in 400 μg/mL and 500 μg/mL were obviously broken into pieces, which proved that M2/IR780@PLGA nanoparticles alone would affect bacterial membrane structure, and also directly destruct bacterial cell membrane when combine with ultrasound. It has been previously reported that IR780, as a sonosensitizer, can generate $^1O_2$ under the stimulation of ultrasound.[51] $_1O_2$ could display bactericidal effect through destroying bacterial membrane integrity.[52] Therefore, we detected $^1O_2$ generation of bacteria treated with M2/IR780@PLGA nanoparticles and ultrasound. As shown in Figure 4C and quantification results in Figure 4A (e), without ultrasound treatment, M2/IR780@PLGA nanoparticles could slightly induce $^1O_2$ generation in bacteria in 200 μg/mL and higher nanoparticle concentration groups. When combined with ultrasound, M2/IR780@PLGA nanoparticles induced dose-dependently $^1O_2$ increase in treated bacteria. It indicated that M2/IR780@PLGA nanoparticles could induce $^1O_2$ generation with the assistance of ultrasound, which would help in destroying bacterial cell integrity. Besides, compared with untreated group,

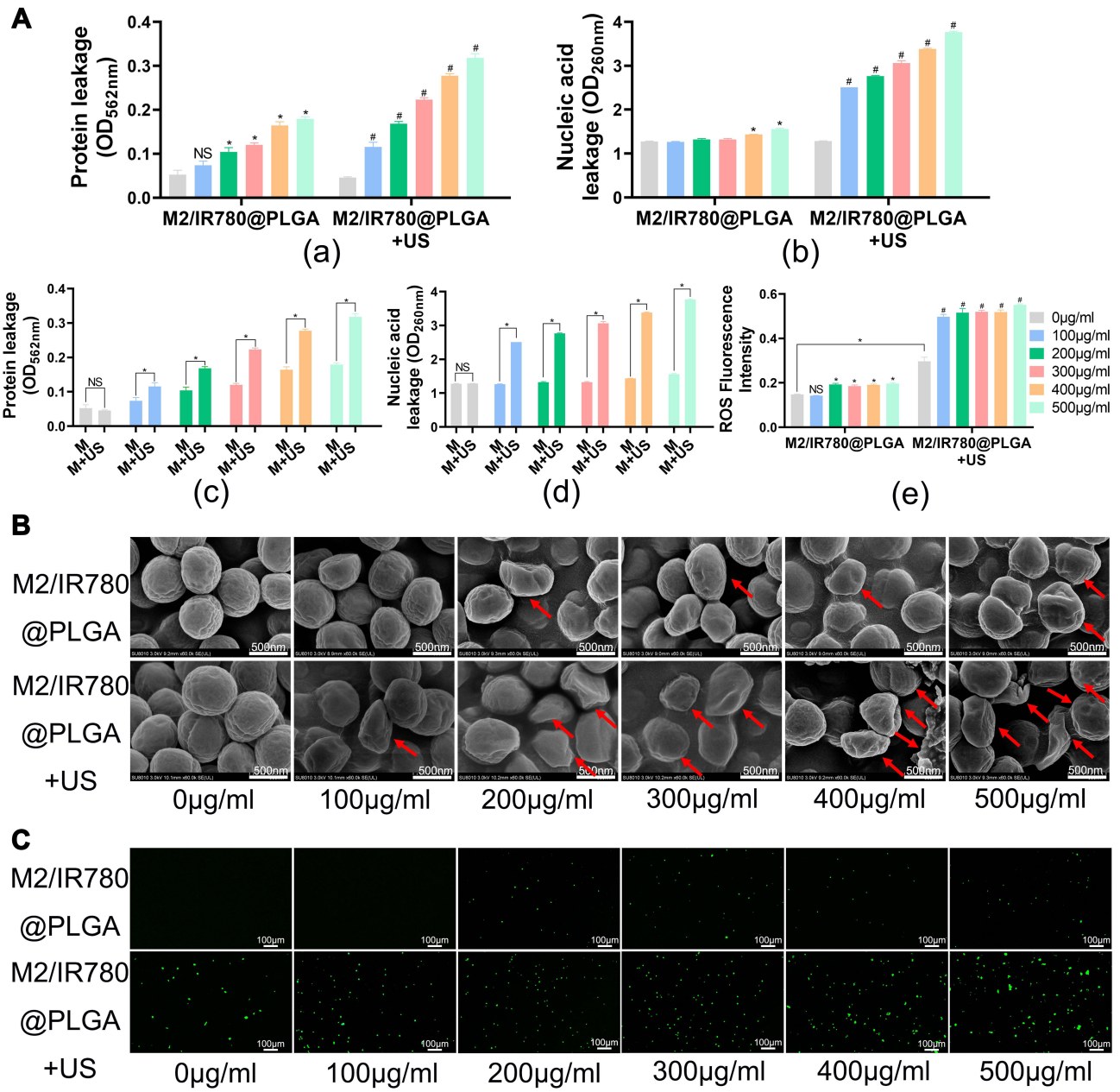

Figure 4 (**A**) The results of protein leakage and nucleic acid leakage after treating ATCC43300 strain with M2/IR780@PLGA nanoparticles, with or without ultrasound. (**B**) presents the SEM results of bacteria treated with M2/IR780@PLGA nanoparticles, with or without ultrasound. (**C**) ROS regeneration of bacteria after treatment with nanoparticles and ultrasound, quantified by ImageJ software and analyzed by One-way ANOVA.

Notes: (**a**) and (**b**) show the leaked protein and nucleic acid amount from bacteria cells treated for 6 hours. (**c**) and (**d**) show comparation of leakage amount between with and without ultrasound treatment groups, under the same administrated nanoparticles concentration in each compared two groups (M: M2/IR780@PLGA). (**e**) presents the quantification results of (**C**). *p < 0.05 means statistically significant difference between M2/IR780@PLGA nanoparticles treated groups and control group; #p < 0.05 means statistically significant difference between M2/IR780@PLGA nanoparticles with ultrasound treated groups and control group. NS means no statistically significant difference between compared groups. Data are expressed as means SD (n = 3).

ultrasound alone group could also raise the $^1O_2$ generation level in bacteria. Given that bacteria kept intact and no difference was observed in cell leakage test between these two groups, we speculated that the induced $^1O_2$ by ultrasound was not enough to influence the integrity of bacterial cell membrane. Figure 4 proves that M2/IR780@PLGA nanoparticles combined with ultrasound could generate $^1O_2$ in treated bacteria, destroy bacterial cell membrane integrity and break ATCC43300 strain into pieces, which could partially explain the mechanism behind nanoparticles bactericidal effect.

Biodistribution of Nanoparticles in Bacterial Infections

For successful treatment, the drug delivery system should accumulate efficiently at the site of inflammation.[53] To assess the gathering ability to bacterial infections position and biodistribution, the NIR fluorescence imaging performance of M2/IR780@PLGA nanoparticles was measured and IR780@PLGA nanoparticles (without M2 macrophage-derived cell membranes) were used as control. IR780 was embedded in PLGA nanoparticles as a sonosensitizer, which could also be used for near-infrared fluorescent tracer. As shown in Figure 5A and B, the fluorescence of the right leg (MRSA-infected site) was extremely stronger than that of left leg (healthy leg) at all time points, owing to the forceful collaboration of the enhanced permeation and retention (EPR) effect at inflammatory site. Additionally, the fluorescence signal of M2/IR780@PLGA nanoparticles decayed more slowly than that of IR780@PLGA nanoparticles, and showed more outstanding accumulation at sites of inflammation at all time points. The fluorescence intensity of M2/IR780@PLGA nanoparticles presented gradual uptrend over time and reached a peak in 24h, while the apex of IR780@PLGA nanoparticles was postponed to 36h, which may demonstrate the targeting ability of M2 macrophage cell membranes to the inflammatory site.[54] Moreover, the fluorescence signal of M2/IR780@PLGA nanoparticles could still be detected until 108h, while IR780@PLGA nanoparticles already had been cleared, manifesting that coating of M2 macrophage cell membranes could prolong circulation time, and it may be crucial for targeting inflammation and retention there through the EPR effect. Therefore, in our subsequent in vivo treatment study, we chose to do administration every 3–4 days, and performed ultrasound therapy within 24 hours of injection. Thereafter, the ex vivo fluorescence intensities of the major organs in the two groups were examined. As shown in Figure 5C and D, most of the NPs gathered in liver due to the enriched reticuloendothelial system (RES) uptake. However, in M2/IR780@PLGA nanoparticles group, the fluorescence intensity of the liver was lower than that in IR780@PLGA nanoparticles group ($p < 0.05$), and a great deal of nanoparticles accumulated at the site of inflammation (right leg), which was 2.3-fold higher than that in IR780@PLGA nanoparticles group ($p < 0.05$), proving that M2 macrophages cell membranes coating could

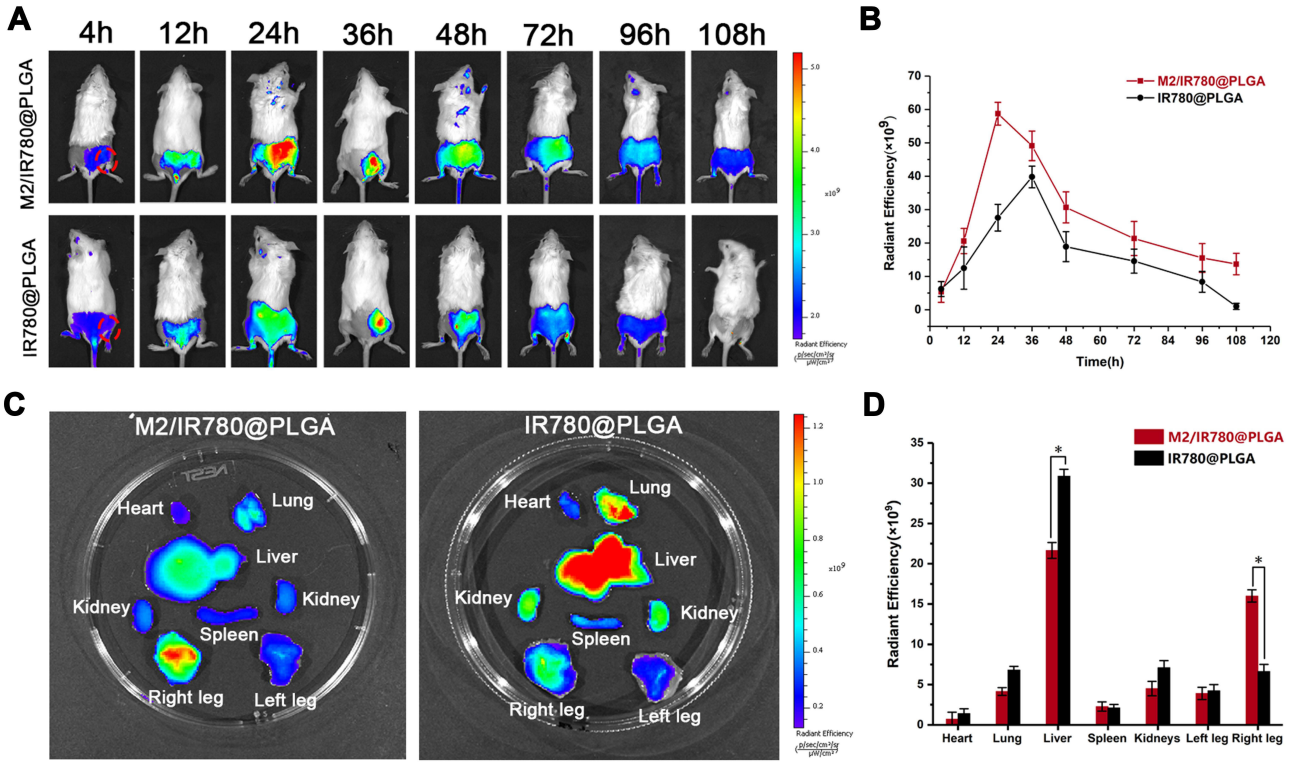

Figure 5 In vivo bacterial myositis targeting ability of M2/IR780@PLGA nanoparticles.

Notes: (**A**) In vivo fluorescence imaging and (**B**) intensities of MRSA infection mice at 4, 12, 24, 36.48, 72, 96, 108 h after intravenous injection of M2/IR780@PLGA nanoparticles or IR780@PLGA nanoparticles. (**C**) Averaged ex vivo NIR fluorescence intensities at 24h and (**D**) NIR fluorescence images of major organs and legs in MRSA infection mice. Data are expressed as means SD (n = 3). Statistical significances were calculated via Student's *t* test, **p* < 0.05.

effectively lower the RES uptake of nanoparticles, tremendously prolong blood circulation, strengthen the EPR in infection and improve the "homing" performance.

Multi-Modal Imaging Monitors the Antibacterial Therapy for Bacterial Infections

To better supervise the therapeutic effect of deep infection, a high-frequency ultrasound instrument was brought in to visualize the therapeutic progress of nanoparticle-mediated SDT. High-frequency ultrasound, with the advantages of high sensitivity, non-invasiveness, non-radiation, convenient inspection and sensitive detection of lesions as small as 2–3mm, is widely used in clinical diagnosis and treatment. A portable high-frequency US was introduced to our study to monitor the infection lesion without therapeutic effect, which could be sterilized and passed through the barrier system to monitor the development of inflammation in mice, thus reducing the restrictions of other detection methods that animals must be taken out of the animal room due to space constraints.[20] B-mode US could visually detect the thickness and swelling of the infected leg through the change of echogenicity, and quantitatively analyze the effect of antibacterial treatment in different treatment groups. CDFI-mode US showed the blood flow signal of the infected lesion, which is usually proportional to the degree of inflammation. In addition, MR images were also used to evaluate the degree of muscular infection. Schematic illustration of in vivo therapeutic and imaging in MRSA infection mice is shown in Figure 6A. The representative B-mode and CDFI-mode US images and MRI images from different treatment groups during observation is displayed in Figure 6B, the leg thickness in the M2/IR780@PLGA + US group was significantly smaller than that in the other three groups, similar to the blood flow signals. After 14 days treatment at different groups, MRI images showed that the right leg of M2/IR780@PLGA + US treated mice only has a slight muscular edema, the right leg of IR780@PLGA + US treated mice has a mild muscular edema, while the right legs of the other two groups (US, saline) have severe muscular edema and obvious intermuscular abscesses, which were also detected by high-frequency ultrasound in US and saline treated groups due to the useless anti-bacterial therapeutic effect by low-frequency US alone or saline (Figure 6C). Then the corresponding quantitative analysis of infected leg (right leg) and normal leg (left leg) circumference measured by US at different time points is shown in Figure 6D and E. Furthermore, the body weight curves showed no obvious weight loss among these groups after different treatments, indicating the good biosafety of these treatments (Figure S7). These results indicated that high-frequency US was a portable, low-cost, reusable and precise apparatus for monitoring small animal experiments, which could efficiently detect muscular inflammation and abscesses with high accuracy and sensitivity. In this study, MR images were also used to access the muscular inflammation with high sensitivity at the last time point; however, the small animals have to be brought out of the experimental barriers when using MR evaluation, which limited its preclinical application in real-time laboratory observation.

The therapeutic effectiveness of M2/IR780@PLGA nanoparticles in SDT was also investigated by HE staining, Giemsa staining, and immunofluorescence examination of muscle tissues harvested from different groups after 14 days. As shown in Figure 7A, treatment with US or saline had no effect on inhibiting MRSA infection, presenting significant deterioration from diffuse muscular edema and focal liquefactive necrosis, and an obvious abscess cavity was generated on HE staining. In the corresponding Giemsa staining, many blue stained clumped bacteria were observed. In addition, coagulative necrosis in muscle tissue on HE staining (the large areas of red staining without structure), with abundant bacteria on Giemsa staining were detected in these two groups (Figure S8). While IR780@PLGA nanoparticles with US irradiation slightly alleviated the infection, no obvious abscess cavities were also observed by HE staining. In contrast, M2/IR780@PLGA nanoparticles combined with US irradiation significantly suppressed mild inflammatory cell infiltration of MRSA infection and without abscess cavities generation. The quantifications of bacteria and inflammatory cells in the infection area were calculated in Figures 7B and S9. These results implied that nanoparticles-mediated SDT has remarkable antibacterial efficacy, especially mediated with the M2/IR780@PLGA nanoparticles due to the M2 macrophages cell membranes coating, which could effectively lower the RES uptake of nanoparticles, tremendously prolong blood circulation and strengthen the EPR in infection, therefore enhancing the SDT effect in the deep-seated infection. Serum biochemical assays for CRP, neutrophil cells and WBC at day 0 and 14 were evaluated for the serum inflammatory levels (Figure 7C). The serum inflammatory levels in day 14 were slightly elevated in US alone and saline groups compared with day 0. By contrast, the serum inflammatory levels in day 14 were significantly reduced compared with day 0 in the nanoparticles-mediated SDT groups,

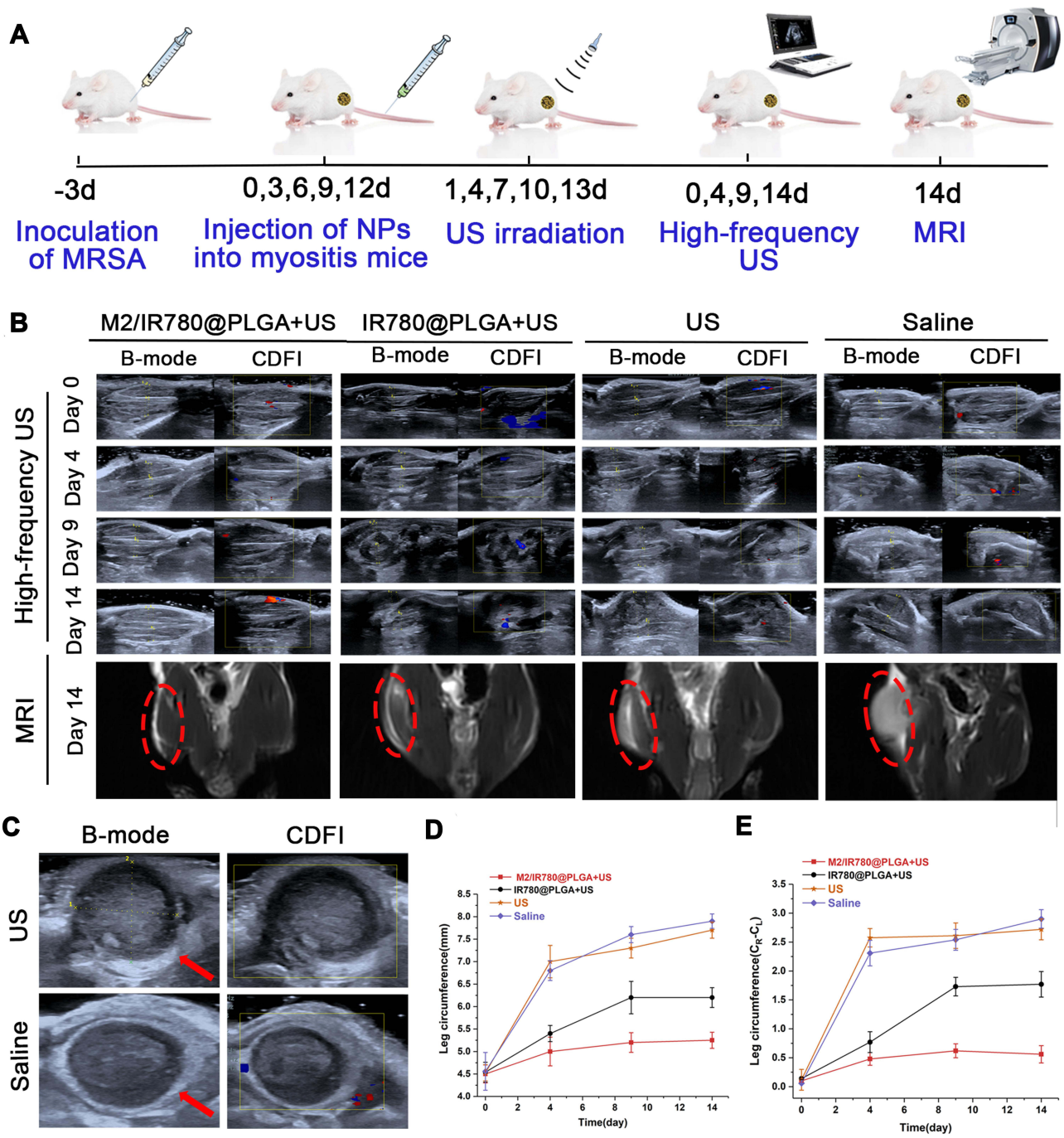

Figure 6 (**A**) Schematic illustration of in vivo therapeutic and imaging in MRSA infection mice. (**B**) Representative high-frequency US and MRI images of the MRSA infected mice within 14 days post-injection in different groups. (**C**) Intermuscular abscess detected by high-frequency ultrasound in US and saline treated groups. (**D**) Average right leg circumference curve and (**E**) the leg circumference relative to the left leg measured by high-frequency US.

Notes: Data are expressed as means SD (n = 3). Statistical significances were calculated via Student's *t* test, $^{*}p < 0.05$.

which indicating the nanoparticles-mediated SDT could definitely alleviate systemic inflammatory response. In contrast of naked IR780@PLGA nanoparticles, M2/IR780@PLGA nanoparticles have a better inhibition efficacy for bacterial growth due to the improved targeting ability of M2 nanoparticles and M1-to-M2 macrophages re-polarization. Immunofluorescence staining of CD206, CD86 and IL-10 have proved the mechanism of M1-to-M2 macrophages re-polarization. Reprogramming macrophages from pro-inflammatory M1 type to anti-inflammatory M2 type is known to efficiently inhibit bacterial infection, the function of macrophages depends on their polarization, which influences their cytokines production

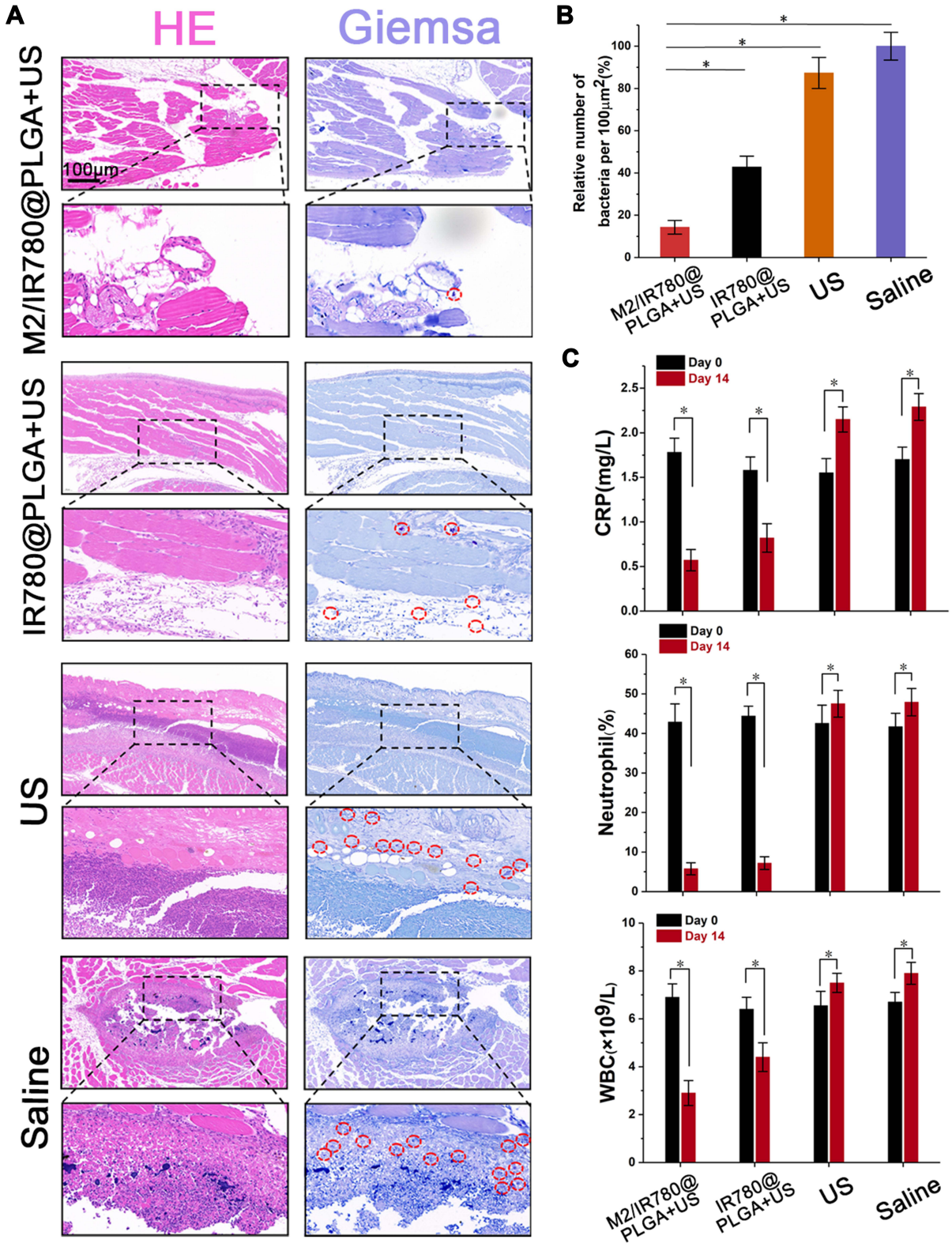

Figure 7 Histomorphological and blood inflammatory factors analysis.

Notes: (**A**) HE and Giemsa staining images of the MRSA infected mice in 14 days post-injection in different groups. In the US and saline groups, the location of the black dashed box in the HE image is the abscess wall. The red circles in the Giemsa image represent the clumped bacteria. Scale bar: 100 μm. (**B**) Quantification of bacteria in the infection area. (**C**) The blood inflammatory factors in 0 and 14 days in different groups. Data are expressed as means SD (n = 3). Statistical significances were calculated via ANOVA, *$p < 0.05$.

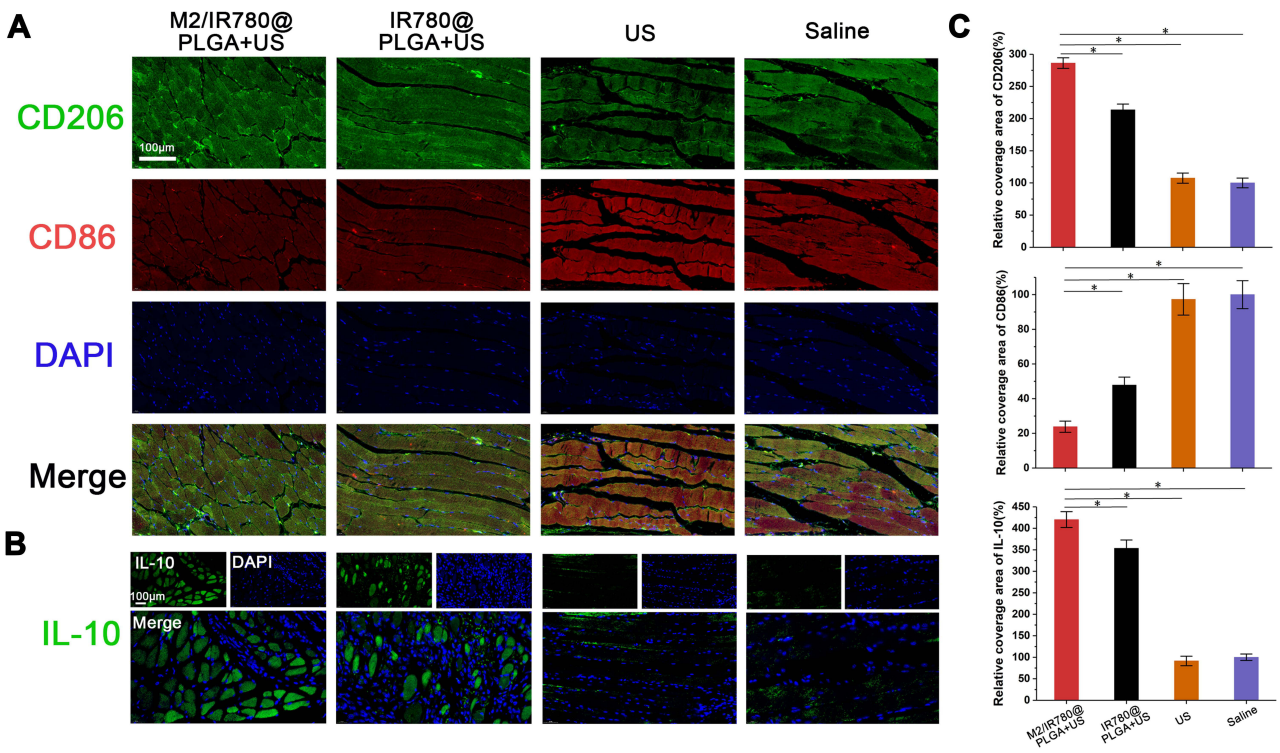

Figure 8 Immunofluorescence analysis.
Notes: (**A** and **B**) Representative immunofluorescence images showing CD206, CD86 and IL-10 in different groups. Scale bar: 100 μm. (**C**) The relative quantification of CD206, CD86 and IL-10 after different treatments. Data are expressed as means SD (n = 3). Statistical significances were calculated via Student's *t* test, $^{*}p < 0.05$.

and their molecules expression on the surface. As shown in Figure 8A and B, green fluorescence labeled CD206 and IL-10 displayed most green fluorescence in the M2/IR780@PLGA nanoparticles-mediated SDT group, slightly less in the IR780@PLGA nanoparticles-mediated SDT group, and rare expression in the US or saline groups. In contrast, red fluorescence labeled CD86 revealed the least red fluorescence in the M2/IR780@PLGA nanoparticles-mediated SDT group, slightly more in the IR780@PLGA nanoparticles-mediated SDT group, and the most expression in the US or saline groups. The relative quantification of CD206, CD86 and IL-10 after different treatments were calculated in Figure 8C. The results indicated that more M2 macrophages expression (CD206 and IL-10 positive, CD86 negative) and less M1 macrophages expression (CD206 and IL-10 negative, CD86 positive) in the M2/IR780@PLGA nanoparticles-mediated SDT group, which means that M2/IR780@PLGA nanoparticles could effectively enhance the antibacterial SDT and subsequent promote M2 macrophages polarization to boost the therapeutic efficacy of MRSA myositis. In this present study, we found that M2/IR780@PLGA nanoparticles significantly downregulated the levels of CD86, and successfully upregulated the levels of CD206 and IL-10, suggesting that the M2/IR780@PLGA nanoparticles can efficiently suppress the formation of M1 type and accomplish a M1-to-M2 switch.

Immune Responses Induced by Antibacterial SDT of MRSA Infections

To evaluate the immune responses triggered by M2/IR780@PLGA nanoparticles-based SDT, dendritic cells in spleens were studied on day 14. It was found that the volume of spleens in the M2/IR780@PLGA nanoparticles-based SDT group was smaller than that of other three groups (Figure 9A and B). Furthermore, as shown in Figure 9C and D, the percentage of mature dendritic cells (CD11c+ CD80+ CD86+) was much higher in the group of mice with M2/IR780@PLGA nanoparticles-based SDT than those of other three groups. These results indicated that the successful establishment of anti-bacterial immune responses triggered by M2/IR780@PLGA nanoparticles-based SDT.

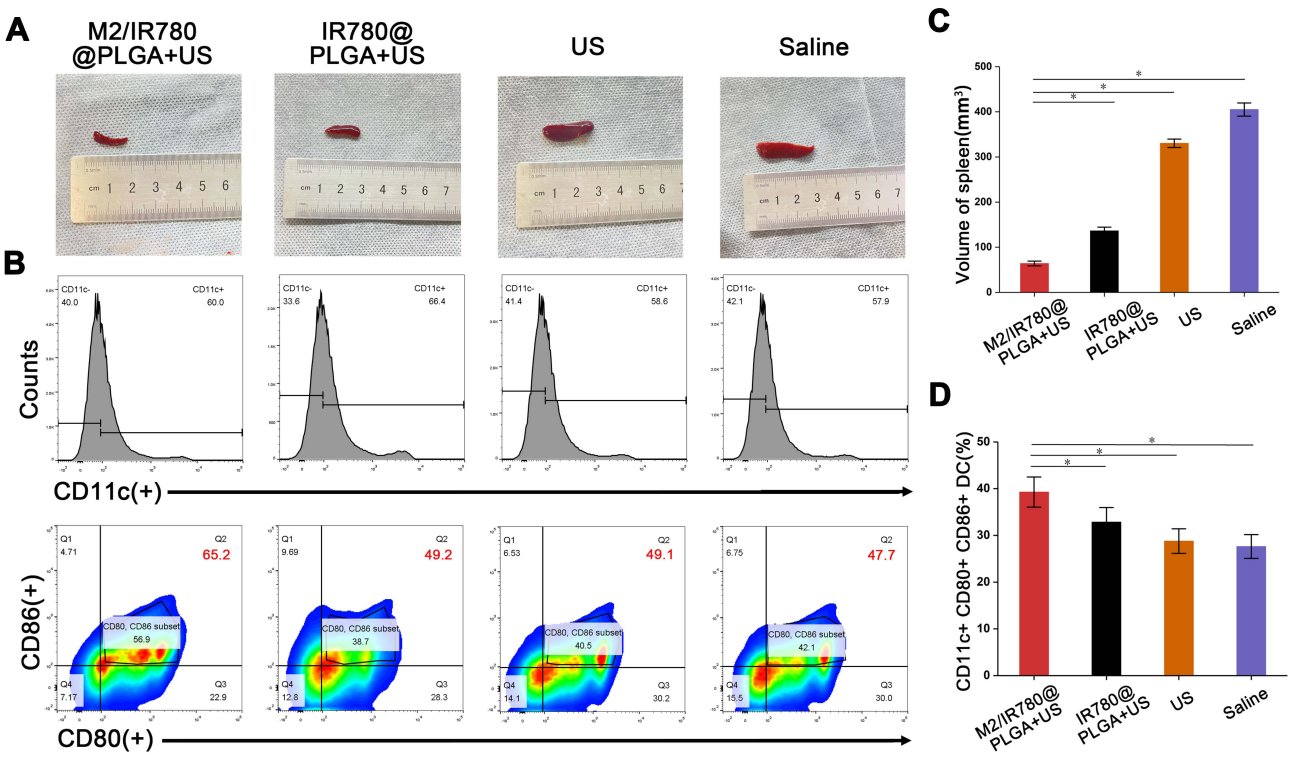

Figure 9 (**A**) General diagram and (**B**) the relative volume of spleens obtained from mice in different treatment groups. (**C, D**) Representative flow cytometry plots (**C**) and quantification (**D**) of CD80 and CD86 expression on dendritic cells gated by CD11c+ cells.
Notes: Data are expressed as means SD (n = 3). Statistical significances were calculated via Student s *t* test. *P < 0.05.

Safety Assessment of M2/IR780@PLGA Nanoparticles

For assessment of the biological toxicity of the developed M2/IR780@PLGA nanoparticles, blood samples were collected for serum biochemistry assays at 14 days after different treatments, including ALT, AST, UREA and CREA. As shown in Figure 10A, the four indicators of hepatic and renal functions have no significant difference between different groups. In addition, after sacrifice of all mice at the 14 days, the major organs were harvested for HE staining to access the histological changes. As shown in Figure 10B, no noticeable organ damage was observed in HE staining sections of major organs in different treatment groups, indicating that the M2/IR780@PLGA nanoparticles have a good biocompatibility with seldom toxic side effects.

However, M2 macrophage membranes manufacturing and quality control need to be addressed before they can be applied in the future clinic. The dosage for clinical use and long-term side effects of these nanoparticles are also required to optimize.

Conclusion

In this study, we reported a M2/IR780@PLGA nanoparticles for antibacterial SDT and subsequent M2 macrophage polarization to enhance the therapeutic efficacy of MRSA myositis, with dual-modal US and MRI monitoring the sono-therapeutic progression. In an MRSA-infected mice model, a great deal of M2/IR780@PLGA nanoparticles accumulated at the site of inflammation. Under high-frequency US and MR images guiding, the infected legs in the M2/IR780@PLGA nanoparticles-based SDT group were significantly smaller, fewer blood flow signals, a slight muscular edema without obvious intermuscular abscesses. Histopathology proved the infected legs in the M2/IR780@PLGA nanoparticles-mediated SDT group had less clumped bacteria infiltration, more M2 macrophage expression and less M1 macrophage expression. The percentage of mature dendritic cells in spleens was much higher in the group of mice with M2/IR780@PLGA nanoparticles-based SDT. Overall, this study provides a promising nanoparticles-based SDT anti-

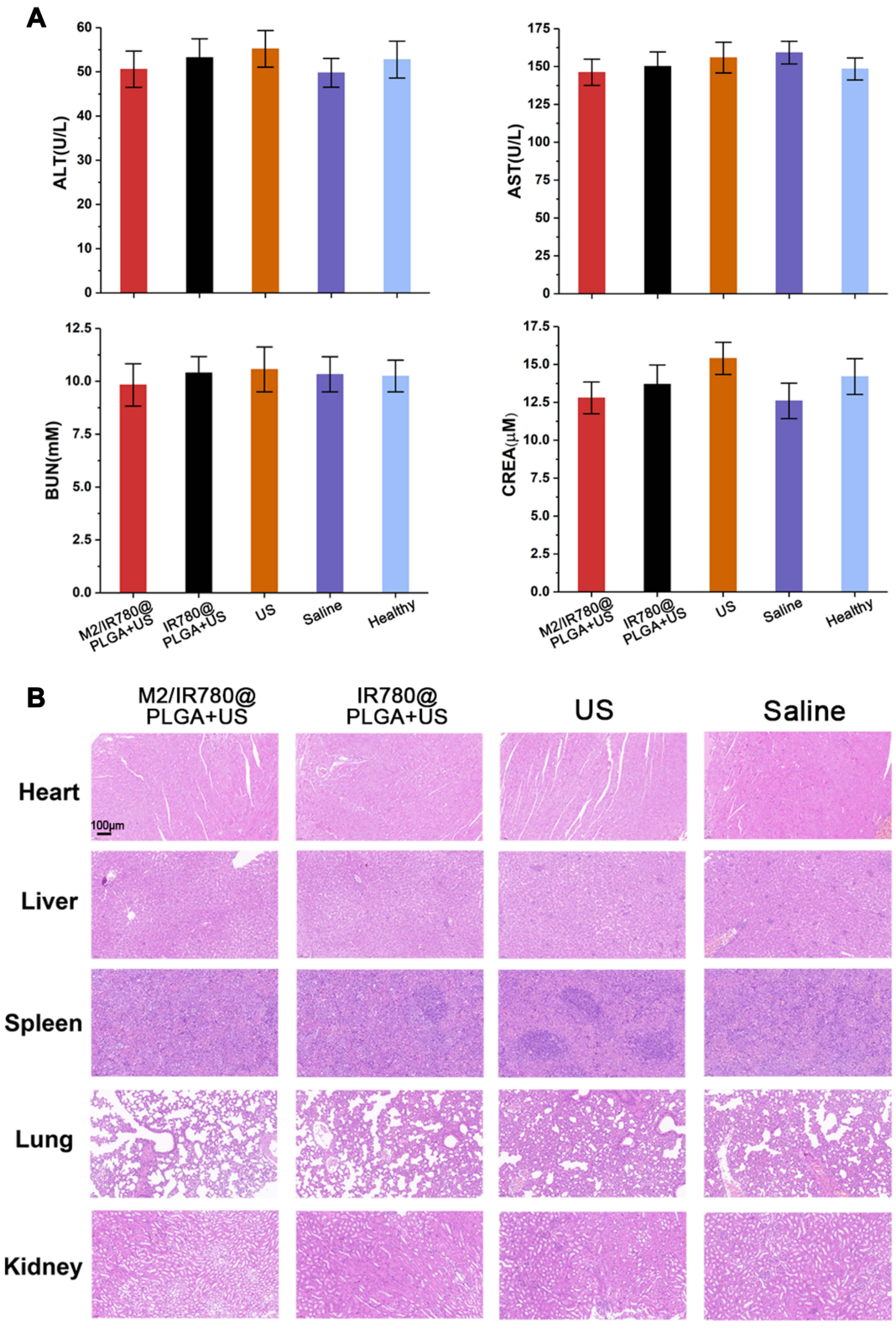

Figure 10 Safety assessment of M2/IR780@PLGA nanoparticles.

Notes: (**A**) Serum biochemistry assays including ALT, AST, BUN and CREA were assessed at 14 days after different treatment, the healthy mice were used as control. (**B**) HE staining images of heart, liver, spleen, lung and kidney at day 14 after different treatments. Scale bar: 100 μm.

bacterial strategy, which could effectively enhance the antibacterial SDT and subsequent promote M2 macrophage polarization to boost the therapeutic efficacy of MRSA myositis.

Abbreviations

MRSA, Methicillin-resistant Staphylococcus aureus; MDR, Multidrug-resistant; SDT, Sonodynamic therapy; US, Ultrasound; ROS, Reactive oxygen species; PDT, Photodynamic therapy; TiO_2, titanium dioxide; IL-4, interleukin-4; TGF-β, transforming growth factor-β; Arg 1, arginase 1; MRI, magnetic resonance imaging; DMEM, Dulbecco's Modified Eagle Medium; CRP, C-reactive protein, WBC, white blood cells; ALT, alanine aminotransferase; AST, aspartate aminotransferase; UREA, urea nitrogen; CREA, creatinine; PVA, polyvinyl alcohol; SOSG, Singlet Oxygen Sensor Green; CCK-8, Cell-Counting Kit-8; DAPI, 4, 6-diamidino-2-phenylindole; PI, pyridine iodide; FBS, fetal bovine serum; RT-PCR, real-time polymerase chain reaction; TEM, transmission electron microscopy; DLS, dynamic light scattering; CLSM, confocal laser scanning microscopy; TSB, tryptic soy broth; SEM, scanning electron microscope; EP, Eppendorf tubes; BCA, Bicin-choninic Acid; MIC, minimum inhibitory concentration.

Data Sharing Statement

All data used to generate these results is available in the main text.

Ethics Approval

All animal experiments were approved by the Ethics Committee of the Second Xiangya Hospital of Central South University.

Author Contributions

All authors made substantial contributions to conception and design, acquisition of data, or analysis and interpretation of data; took part in drafting the article or revising it critically for important intellectual content; agreed to submit to the current journal; gave final approval of the version to be published; and agree to be accountable for all aspects of the work.

Funding

This project was funded by the National Natural Science Foundation of China (81974267), Science and Technology Innovation Program of Hunan Province (2021RC3033) and Hunan Provincial Natural Science Foundation of China (2022JJ30827).

Disclosure

The authors report no conflicts of interest in this work.

References

1. Lee AS, de Lencastre H, Garau J., et al. Methicillin-resistant Staphylococcus aureus. *Nat Rev Dis Primers*. 2018;4:18033. doi:10.1038/nrdp.2018.33
2. Turner NA, Sharma-Kuinkel BK, Maskarinec SA, et al. Methicillin-resistant Staphylococcus aureus: an overview of basic and clinical research. *Nat Rev Microbiol*. 2019;17(4):203–218. doi:10.1038/s41579-018-0147-4
3. Xu S, Chang L, Hu Y, et al. Tea polyphenol modified, photothermal responsive and ROS generative black phosphorus quantum dots as nanoplatforms for promoting MRSA infected wounds healing in diabetic rats. *J Nanobiotechnology*. 2021;19(1):362. doi:10.1186/s12951-021-01106-w
4. Chait R, Craney A, Kishony R. Antibiotic interactions that select against resistance. *Nature*. 2007;446(7136):668–671. doi:10.1038/nature05685
5. Zhang Q, Lambert G, Liao D, et al. Acceleration of emergence of bacterial antibiotic resistance in connected microenvironments. *Science*. 2011;333(6050):1764–1767. doi:10.1126/science.1208747
6. Zhao Y, Guo Q, Dai X, et al. A biomimetic non-antibiotic approach to eradicate drug-resistant infections. *Adv Mater*. 2019;31(7):e1806024. doi:10.1002/adma.201806024
7. Mei Z, Gao D, Hu D, et al. Activatable NIR-II photoacoustic imaging and photochemical synergistic therapy of MRSA infections using miniature Au/Ag nanorods. *Biomaterials*. 2020;251:120092. doi:10.1016/j.biomaterials.2020.120092
8. Zhao X, Chang L, Hu Y, et al. Preparation of photocatalytic and antibacterial MOF nanozyme used for infected diabetic wound healing. *ACS Appl Mater Interfaces*. 2022;14(16):18194–18208. doi:10.1021/acsami.2c03001
9. Ren X, Hu Y, Chang L, Xu S, Mei X, Chen Z. Electrospinning of antibacterial and anti-inflammatory Ag@hesperidin core-shell nanoparticles into nanofibers used for promoting infected wound healing. *Regen Biomater*. 2022;9:rbac012. doi:10.1093/rb/rbac012

10. Ren X, Lv X, Chen Z, Zhang P, Hu X, Mei X. Preparation of Ag nanoclusters-modified non-sintered silica ceramic-like nanosheet for removing dyes and bacteria from water. *Int J Nanomedicine*. 2021;16:895–904. doi:10.2147/IJN.S286406
11. Pang X, Xiao Q, Cheng Y, et al. Bacteria-responsive nanoliposomes as smart sonotheranostics for multidrug resistant bacterial infections. *ACS Nano*. 2019;13(2):2427–2438. doi:10.1021/acsnano.8b09336
12. Huang B, Chen S, Pei W, et al. Oxygen-sufficient nanoplatform for chemo-sonodynamic therapy of hypoxic tumors. *Front Chem*. 2020;8:358. doi:10.3389/fchem.2020.00358
13. Qian X, Zheng Y, Chen Y. Micro/Nanoparticle-Augmented Sonodynamic Therapy (SDT): breaking the depth shallow of photoactivation. *Adv Mater*. 2016;28(37):8097–8129. doi:10.1002/adma.201602012
14. Pang X, Xu C, Jiang Y, Xiao Q, Leung AW. Natural products in the discovery of novel sonosensitizers. *Pharmacol Ther*. 2016;162:144–151. doi:10.1016/j.pharmthera.2015.12.004
15. Wang X, Ip M, Leung AW, Xu C. Sonodynamic inactivation of methicillin-resistant Staphylococcus aureus in planktonic condition by curcumin under ultrasound sonication. *Ultrasonics*. 2014;54(8):2109–2114. doi:10.1016/j.ultras.2014.06.017
16. Wang X, Ip M, Leung AW, et al. Sonodynamic action of curcumin on foodborne bacteria Bacillus cereus and Escherichia coli. *Ultrasonics*. 2015;62:75–79. doi:10.1016/j.ultras.2015.05.003
17. Leung AW, Ip M, Xu CS, Wang XN, Yung PT, Hua HY. Sonodynamic bactericidal efficacy of hypocrellin A and B against methicillin-resistant Staphylococcus aureus. *Hong Kong Med J*. 2017;23(4):36–37.
18. Li Y, Zhou Q, Deng Z, et al. IR-780 dye as a sonosensitizer for sonodynamic therapy of breast tumor. *Sci Rep*. 2016;6:25968. doi:10.1038/srep25968
19. Wang L, Niu C. IR780-based nanomaterials for cancer imaging and therapy. *J Mater Chem B*. 2021;9(20):4079–4097. doi:10.1039/D1TB00407G
20. Huang B, Wang L, Tang K, et al. IR780 based sonotherapeutic nanoparticles to combat multidrug-resistant bacterial infections. *Front Chem*. 2022;10:840598. doi:10.3389/fchem.2022.840598
21. Hu Y, Huang S, Zhao X, et al. Preparation of photothermal responsive and ROS generative gold nanocages for cancer therapy. *Chem Eng J*. 2021;421:129744. doi:10.1016/j.cej.2021.129744
22. Chang L, Huang S, Zhao X, et al. Preparation of ROS active and photothermal responsive hydroxyapatite nanoplatforms for anticancer therapy. *Mater Sci Eng C Mater Biol Appl*. 2021;125:112098. doi:10.1016/j.msec.2021.112098
23. DeNardo DG, Ruffell B. Macrophages as regulators of tumour immunity and immunotherapy. *Nat Rev Immunol*. 2019;19(6):369–382. doi:10.1038/s41577-019-0127-6
24. Si J, Shao S, Shen Y, Wang K. Macrophages as active nanocarriers for targeted early and adjuvant cancer chemotherapy. *Small*. 2016;12(37):5108–5119. doi:10.1002/smll.201601282
25. Kumar M, Coburn J, Kaplan DL, Mandal BB. Immuno-informed 3D silk biomaterials for tailoring biological responses. *ACS Appl Mater Interfaces*. 2016;8(43):29310–29322. doi:10.1021/acsami.6b09937
26. Li J, Zhao M, Sun M, et al. Multifunctional nanoparticles boost cancer immunotherapy based on modulating the immunosuppressive tumor microenvironment. *ACS Appl Mater Interfaces*. 2020;12(45):50734–50747. doi:10.1021/acsami.0c14909
27. Choo YW, Kang M, Kim HY, et al. M1 macrophage-derived nanovesicles potentiate the anticancer efficacy of immune checkpoint inhibitors. *ACS Nano*. 2018;12(9):8977–8993. doi:10.1021/acsnano.8b02446
28. Wang P, Wang H, Huang Q, et al. Exosomes from M1-polarized macrophages enhance paclitaxel antitumor activity by activating macrophages-mediated inflammation. *Theranostics*. 2019;9(6):1714–1727. doi:10.7150/thno.30716
29. Wang Y, Lin YX, Qiao SL, et al. Polymeric nanoparticles promote macrophage reversal from M2 to M1 phenotypes in the tumor microenvironment. *Biomaterials*. 2017;112:153–163. doi:10.1016/j.biomaterials.2016.09.034
30. Qiu N, Wang G, Wang J, et al. Tumor-associated macrophage and tumor-cell dually transfecting polyplexes for efficient interleukin-12 cancer gene therapy. *Adv Mater*. 2021;33(2):e2006189. doi:10.1002/adma.202006189
31. Mantovani A, Sozzani S, Locati M, Allavena P, Sica A. Macrophage polarization: tumor-associated macrophages as a paradigm for polarized M2 mononuclear phagocytes. *Trends Immunol*. 2002;23(11):549–555. doi:10.1016/S1471-4906(02)02302-5
32. van der Zande HJP, Nitsche D, Schlautmann L, Guigas B, Burgdorf S. The Mannose Receptor: from endocytic receptor and biomarker to regulator of (meta)inflammation. *Front Immunol*. 2021;12:765034. doi:10.3389/fimmu.2021.765034
33. Hu CMJ. Nanoparticle biointerfacing by platelet membrane cloaking. *Nature*. 2015;1;526.
34. Thamphiwatana S. Macrophage-like nanoparticles concurrently absorbing endotoxins and proinflammatory cytokines for sepsis management. *Proc Natl Acad Sci USA*. 2017;2:114.
35. Zhang QZ, Dehaini D, Zhang Y, et al. Neutrophil membrane-coated nanoparticles inhibit synovial inflammation and alleviate joint damage in inflammatory arthritis. *Nat Nanotechnol*. 2018;13(12):1182. doi:10.1038/s41565-018-0254-4
36. Wang L, Chen S, Pei W, Huang B, Niu C. Magnetically targeted erythrocyte membrane coated nanosystem for synergistic photothermal/chemotherapy of cancer. *J Mater Chem B*. 2020;8(18):4132–4142. doi:10.1039/D0TB00364F
37. Pei W, Huang B, Chen S, Wang L, Xu Y, Niu C. Platelet-mimicking drug delivery nanoparticles for enhanced chemo-photothermal therapy of breast cancer. *Int J Nanomedicine*. 2020;15:10151–10167. doi:10.2147/IJN.S285952
38. Li H, Feng Y, Zheng X, et al. M2-type exosomes nanoparticles for rheumatoid arthritis therapy via macrophage re-polarization. *J Control Release*. 2022;341:16–30. doi:10.1016/j.jconrel.2021.11.019
39. Yu Y, Li J, Zhang Y, et al. A bioinspired hierarchical nanoplatform targeting and responding to intracellular pathogens to eradicate parasitic infections. *Biomaterials*. 2022;280:121309. doi:10.1016/j.biomaterials.2021.121309
40. Wu G, Zhang J, Zhao Q, et al. Molecularly engineered macrophage-derived exosomes with inflammation tropism and intrinsic heme biosynthesis for atherosclerosis treatment. *Angew Chem Int Ed Engl*. 2020;59(10):4068–4074. doi:10.1002/anie.201913700
41. Pei W, Li X, Bi R, et al. Exosome membrane-modified M2 macrophages targeted nanomedicine: treatment for allergic asthma. *J Control Release*. 2021;338:253–267. doi:10.1016/j.jconrel.2021.08.024
42. Wang L, Chen S, Zhu Y, et al. Triple-Modal imaging-guided chemo-photothermal synergistic therapy for breast cancer with magnetically targeted phase-shifted nanoparticles. *ACS Appl Mater Interfaces*. 2018;10(49):42102–42114. doi:10.1021/acsami.8b16323
43. Chen S, Huang B, Pei W, Wang L, Xu Y, Niu C. Mitochondria-targeting oxygen-sufficient perfluorocarbon nanoparticles for imaging-guided tumor phototherapy. *Int J Nanomedicine*. 2020;15:8641–8658. doi:10.2147/IJN.S281649

44. Wang L, Chen SJ, Zhu Y, et al. Triple-modal imaging-guided chemo-photothermal synergistic therapy for breast cancer with magnetically targeted phase-shifted nanoparticles. *Acs Appl Mater Inter*. 2018;10(49):42102–42114.
45. Tan H, Peng Z, Li Q, Xu X, Guo S, Tang T. The use of quaternised chitosan-loaded PMMA to inhibit biofilm formation and downregulate the virulence-associated gene expression of antibiotic-resistant staphylococcus. *Biomaterials*. 2012;33(2):365–377. doi:10.1016/j.biomaterials.2011.09.084
46. Allkja J, Bjarnsholt T, Coenye T, et al. Minimum information guideline for spectrophotometric and fluorometric methods to assess biofilm formation in microplates. *Biofilm*. 2020;2:100010. doi:10.1016/j.bioflm.2019.100010
47. Wang Q, Zhang W, Peng X, et al. GSK-3beta suppression upregulates Gli1 to alleviate osteogenesis inhibition in titanium nanoparticle-induced osteolysis. *J Nanobiotechnology*. 2022;20(1):148. doi:10.1186/s12951-022-01351-7
48. Chen Q, Xu L, Liang C, Wang C, Peng R, Liu Z. Photothermal therapy with immune-adjuvant nanoparticles together with checkpoint blockade for effective cancer immunotherapy. *Nat Commun*. 2016;7:13193. doi:10.1038/ncomms13193
49. Guan D, Chen F, Qiu Y, et al. Sulfonium, an underestimated moiety for structural modification, alters the antibacterial profile of vancomycin against multidrug-resistant bacteria. *Angew Chem Int Ed Engl*. 2019;58(20):6678–6682. doi:10.1002/anie.201902210
50. Li Y, Zhao J, Zhang G, et al. Visible-light-driven photocatalytic disinfection mechanism of Pb-BiFeO3/rGO photocatalyst. *Water Res*. 2019;161:251–261. doi:10.1016/j.watres.2019.06.011
51. Zhang L, Yi H, Song J, et al. Mitochondria-targeted and ultrasound-activated nanodroplets for enhanced deep-penetration sonodynamic cancer therapy. *ACS Appl Mater Interfaces*. 2019;11(9):9355–9366. doi:10.1021/acsami.8b21968
52. Ezraty B, Gennaris A, Barras F, Collet JF. Oxidative stress, protein damage and repair in bacteria. *Nat Rev Microbiol*. 2017;15(7):385–396. doi:10.1038/nrmicro.2017.26
53. Kim J, Kim HY, Song SY, et al. Synergistic oxygen generation and reactive oxygen species scavenging by manganese ferrite/ceria co-decorated nanoparticles for rheumatoid arthritis treatment. *ACS Nano*. 2019;13(3):3206–3217. doi:10.1021/acsnano.8b08785
54. Maeda H. The link between infection and cancer: tumor vasculature, free radicals, and drug delivery to tumors via the EPR effect. *Cancer Sci*. 2013;104(7):779–789. doi:10.1111/cas.12152